R. & M. No. 2662
(21,526)
A.R.C. Technical Report

MINISTRY OF SUPPLY

AERONAUTICAL RESEARCH COUNCIL
REPORTS AND MEMORANDA

Corrections to Velocity for Wall Constraint in any 10 × 7 Rectangular Subsonic Wind Tunnel

By

J. Y. G. Evans, B.Sc.

LONDON: HER MAJESTY'S STATIONERY OFFICE
1953
PRICE 12*s* 6*d* NET

Corrections to Velocity for Wall Constraint in any 10 × 7 Rectangular Subsonic Wind Tunnel

By

J. Y. G. Evans, B.Sc.

Communicated by the Principal Director of Scientific Research (Air), Ministry of Supply

Reports and Memoranda No. 2662*

April, 1949

Summary.—The validity and accuracy of methods of determining corrections to the measured velocity in a wind tunnel to compensate for the constraining effect of the walls are reviewed following recent experimental evidence from the R.A.E. 10 × 7 ft subsonic wind tunnel. It is concluded that such corrections, commonly known as 'blockage' corrections, can be successfully applied at Mach numbers up to 0·96 but some modifications are necessary to the formulae at present in use. The more important of these are outlined below.

(1) The compressibility factor should be based on the corrected Mach number of the stream.

(2) The ratio of 'solid' blockage (*i.e.*, the blockage due to model excluding wake) to the peak wall velocity increment is not constant but depends on the length of the model and the Mach number of the stream.

(3) The calculated solid blockage of a wing must be increased to allow for the presence of local supersonic flow. For wings of usual plan form, this may be done by an empirical factor which is a function of the rise in drag coefficient.

(4) Addition of corner fillets to the tunnel gives rise to a larger percentage increase of the solid blockage than of the wall velocity increments.

Formulae for the calculation of the longitudinal distribution of blockage increment due to any model, necessary to check the validity of the method in particular cases, are presented in a form which, it is hoped, will facilitate their use in any 10 × 7 wind tunnel. Formulae for the corresponding wall velocity increments, used to check the accuracy of the method by comparison with measured wall pressures, are also given.

1. *Introduction.*—Formulae for the application of 'blockage' corrections to velocity measurements in the Royal Aircraft Establishment 10 × 7 ft High Speed Tunnel were first set up by Thom in 1943[1] and this method of allowing for the constraining effect of the walls has been in use, with little modification, up to the present time[2]. The theory is based on the principle that the constraining effect of the walls is similar to that of an infinite array of images of the model in the walls. The induced velocity at the model due to these images has been calculated for incompressible flow by the usual potential theory and allowance for compressibility made according to the standard linear perturbation theory, scaling up the incompressible flow values by $(1 - M_U^2)^{-n/2}$, where M_U is the empty tunnel Mach number for the same upstream conditions, and n is an integer.

The usual method of representation of the model and wake by a simple source and sink system for the purpose of calculating the velocity field in compressible flow is not exact and requires theoretical and experimental backing. Very little experimental evidence has been available because the additional complication of any supporting system in the plane of the model makes a measurement of the true model blockage extremely difficult.

* R.A.E. Report Aero. 2307, received 18th August, 1949.

Recently an alternative method of testing complete models has been developed in which the model is supported by a small sting from the rear (*e.g.*, Fig. 23) and a variety of models have now been tested by this method at Mach numbers up to 0·95. The data obtained from wall pressure measurements during these tests, together with the results of some special tests on bodies of the same shape but different sizes, are used in the present paper to examine the accuracy and validity of the accepted theory.

It was evident at an early stage that some of the simplifications in theory which led to Thom's formulae were not entirely justified. In consequence, the theory has been rewritten, in section 2 below, in a more general form and a more elaborate set of blockage formulae has been obtained. Modifications to these formulae, on an empirical basis, have been made where suggested by the experimental data.

2. *General Theory.*—2.1. *Blockage and Wall Velocity Increment due to a Source in a Rectangular Wind Tunnel.*—Referring to a co-ordinate system as defined in Fig. 1, for incompressible flow in a rectangular wind tunnel ($B \times 0{\cdot}7B$), the increment in longitudinal velocity at a point $A\,(x_0, 0, 0)$ in the tunnel due to wall constraint on a source δq_i at (x, y, z) is given by

$$\Delta_A u = \frac{(x_0 - x)\,\delta q_i}{4\pi B^3} \sum_{m=-\infty}^{+\infty} \sum_{n=-\infty}^{+\infty} \left\{ \left(\frac{x_0 - x}{B}\right)^2 + \left[m + (-1)^m \frac{y}{B}\right]^2 + \left[0{\cdot}7n + (-1)^n \frac{z}{B}\right]^2 \right\}^{-3/2} \quad (1)$$

omitting the term $m = n = 0$. This expression is simply obtained on the principle that the constraining effect can be represented by an infinite array of images of the source in the walls of the tunnel.

A method of modifying equation (1) to make it applicable to compressible flow, provided the incremental velocities are small compared with a basic stream velocity, U, is given by the linear perturbation theory for axi-symmetrical compressible flow. By this theory, the velocity potential due to the source, δq_i, in incompressible flow

$$\Phi_i = -\frac{\delta q_i}{4\pi} \left\{x^2 + r^2\right\}^{-1/2}, \quad (r^2 = y^2 + z^2), \quad \ldots\ldots\ldots\ldots\ldots\ldots \quad (2)$$

which was used to obtain equation (1), becomes in compressible flow

$$\Phi = -\frac{\delta q}{4\pi} \left\{x^2 + \beta^2 r^2\right\}^{-1/2} \quad \ldots\ldots\ldots\ldots\ldots\ldots\ldots\ldots \quad (3)$$

where $\delta q\ (= \delta q_i/\beta^2)$ is the volume flow and $\beta^2 = 1 - M^2$, where M is a basic stream Mach number. Thom and most later investigators have used the Mach number, M_u, measured in the empty tunnel at the same upstream conditions. It will be shown below (*e.g.*, section 5.2) that better agreement with experimental evidence is obtained by using the corrected Mach number (*i.e.*, the Mach number corresponding to a velocity $U + \Delta_A u$), which is equivalent to considering the effect of each image of the model in the presence of all others. The corrected Mach number has been used to determine β factors throughout this paper unless expressly stated otherwise.

Applying equation (3), the velocity increment in compressible flow at a point $A(x_0, 0, 0)$ on the tunnel axis due to the images of a source δq at (x, y, z) is given by

$$\Delta_A u = \frac{(x_0 - x)\,\delta q}{4\pi B^3 \beta^3} \sum_{m=-\infty}^{+\infty} \sum_{n=-\infty}^{+\infty} \left\{ \left(\frac{x_0 - x}{\beta B}\right)^2 + \left[m + (-1)^m \frac{y}{B}\right]^2 + \left[0{\cdot}7n + (-1)^n \frac{z}{B}\right]^2 \right\}^{-3/2} \quad (4)$$

omitting the term $m = n = 0$

$$= \frac{\delta q}{4\pi B^3 \beta^3} (x_0 - x) K_A \quad \ldots\ldots\ldots\ldots\ldots\ldots\ldots\ldots \quad (5)$$

Values of K_A and $[(x_0 - x)/\beta B]K_A$ plotted against $[(x_0 - x)/\beta B]$ at constant values of (y/B) and $(z/B) = 0$ are given in Fig. 2.

Similarly, the velocity increments in compressible flow at a point B $(x_0, 0{\cdot}5B, 0)$ on the centre-line of the side wall and at a point C $(x_0, 0, 0{\cdot}35B)$ on the centre-line of the top wall due to a source element δq at (x, y, z) and its images are given respectively by

$$\Delta_B u = \frac{(x_0 - x)\,\delta q}{4\pi B^3 \beta^3} \sum_{m=-\infty}^{+\infty} \sum_{n=-\infty}^{+\infty} \left\{ \left(\frac{x_0 - x}{\beta B}\right)^2 + \left[m - 0{\cdot}5 + (-1)^m \frac{y}{B}\right]^2 + \left[0{\cdot}7n + (-1)^n \frac{z}{B}\right]^2 \right\}^{-3/2} \quad .. \quad .. \quad .. \quad .. \quad .. \quad (6)$$

$$= \frac{\delta q}{4\pi B^3 \beta^3} (x_0 - x) K_B \; .. \quad .. \quad .. \quad .. \quad .. \quad .. \quad .. \quad (7)$$

and

$$\Delta_C u = \frac{(x_0 - x)\,\delta q}{4\pi B^3 \beta^3} \sum_{m=-\infty}^{+\infty} \sum_{n=-\infty}^{+\infty} \left\{ \left(\frac{x_0 - x}{\beta B}\right)^2 + \left[m + (-1)^m \frac{y}{B}\right]^2 + \left[0{\cdot}7n - 0{\cdot}35 + (-1)^n \frac{z}{B}\right]^2 \right\}^{-3/2} \quad .. \quad .. \quad .. \quad .. \quad (8)$$

$$= \frac{\delta q}{4\pi B^3 \beta^3} (x_0 - x) K_C \; .. \quad .. \quad .. \quad .. \quad .. \quad .. \quad .. \quad (9)$$

Values of K_B and K_C plotted against $(x_0 - x)/\beta B$ at constant values of (y/B) and $(z/B) = 0$ are given in Figs. 3 and 4.

From the data of Figs. 2, 3 and 4 it is possible to calculate the longitudinal distribution of blockage and wall increments in velocity due to any shape of wing, body or wake which can be represented by a source distribution in the (x, y)-plane. In practice, however, integration of the contributions from each source element, even by graphical means, is a lengthy process and it is desirable to make a generalised integration giving the velocity increments in terms of relatively simple geometric properties of the model. It has been stated (*e.g.*, Ref. 2) that, for this purpose, both bodies and wings of finite span can be represented by a doublet (*i.e.*, an equivalent sphere). Although this representation is satisfactory in determining the peak centre-line blockage, (in the sense that when the doublet representation fails the gradients in Mach number are usually large enough to invalidate the whole principle of a single blockage correction), it will be shown below that rather more elaborate methods are necessary in determining the gradient in Mach number over the model and in calculating the ratios of blockage increment to wall increment.

2.2. *Representation of a Body or Nacelle.*—A thin body in a uniform stream of velocity U can be represented approximately by a line of sources on the axis of the body, any element of which is given by

$$\delta q = U \frac{dA}{dx}\left(1 + 0{\cdot}4\beta \frac{d}{l}\right) \delta x \quad .. \quad .. \quad .. \quad .. \quad .. \quad .. \quad (10)$$

where (dA/dx) is the local rate of change of cross-sectional area of the body and l/d is the fineness ratio. The factor $[1 + 0{\cdot}4\beta\,(d/l)]$ has been included as a rough method of allowing for the finite thickness of the body and is based on the empirical relationship put forward in Appendix A of Ref. 2.

The blockage at $(x_0, 0, 0)$ due to a body lying along an axis $(y = y', z = 0)$ is then given by equations (5) and (10) as

$$\frac{\Delta_A u}{U} = \frac{\left(1 + 0{\cdot}4\beta \frac{d}{l}\right)}{4\pi B^3 \beta^3} \int (x_0 - x) \frac{dA}{dx} K_{A\left(\frac{x_0 - x}{\beta B},\ \frac{y'}{B},\ 0\right)} dx \quad .. \quad .. \quad .. \quad (11)$$

the integral being taken along the length of the body.

(52308)

Although useful for investigation in particular cases, equation (11) is unnecessarily complicated for routine blockage estimates and it will be shown below that for the latter it is sufficient to represent the body by a source, q, at $(x' - \bar{x}, y', 0)$ and a sink, $-q$, at $(x' + \bar{x}, y', 0)$, where $(x', y', 0)$ is the centre of volume of the body. We then have, from integration of equation (10)

$$2q\bar{x} = U\left(1 + 0{\cdot}4\beta\frac{d}{l}\right)\int x\frac{dA}{dx}\,dx$$

$$= UV\left(1 + 0{\cdot}4\beta\frac{d}{l}\right) \quad .. \quad .. \quad .. \quad .. \quad .. \quad .. \quad .. \quad (12)$$

where V is the volume of the body and, from equations (11) and (12)

$$\frac{\Delta_A u}{U} = \frac{\left(V(1+0{\cdot}4\beta\frac{d}{l}\right)}{4\pi B^3\beta^3}\left\{\frac{(x_0 - x' + \bar{x})K_A\left(\frac{x_0 - x' + \bar{x}}{\beta B}, \frac{y'}{B}, 0\right) - (x_0 - x' - \bar{x})K_A\left(\frac{x_0 - x' - \bar{x}}{\beta B}, \frac{y'}{B}, 0\right)}{2\bar{x}}\right\} \quad .. \quad (13)$$

Values of $\bar{x}$ can be obtained either by fitting the best Rankine ovoid or, more generally, by

$$\bar{x} = \sqrt{3}k_2\,, \quad .. \quad .. \quad .. \quad .. \quad .. \quad .. \quad .. \quad .. \quad (14)$$

where k_2 is the minimum radius of gyration about an axis in the (y, z)-plane (*see* Appendix A).

Corresponding increments in velocity on the walls at B and C are given by equations of form similar to equation (13) in which K_A is replaced by K_B and K_C respectively.

The calculated longitudinal distributions of blockage and wall increments in Mach number for a body (of shape similar to body No. 1 of Fig. 22) under two typical conditions in which large corrections might be expected, namely a model of length $0{\cdot}6B$ at $M = 0{\cdot}85$ and a model of length $0{\cdot}33B$ at $M = 0{\cdot}94$, are shown in Figs. 5 and 6. The calculations have been made by representing the body, in turn, by a continuous source distribution (equation 11), by a source and a sink (equation (13)) and by a doublet. It can be seen that the source and sink give a satisfactory approximation whereas the simpler doublet representation over-estimates both the peak increments and the magnitude of longitudinal gradients in Mach number over the model.

In practice, the peak value of the blockage correction is required, since this determines the equivalent free-stream Mach number for the thickest, and usually most critical, region of the model. The longitudinal gradients are evaluated only at the upper limit of the tests to investigate whether the use of a single blockage correction is still valid. The peak blockage correction can be estimated more easily from the data given in Fig. 7 where

$$(K_A)_{\max} = K_A\left(\frac{\bar{x}}{\beta B}, 0, 0\right)$$

is plotted against Mach number at constant values of $\bar{x}/B$ to give

$$\left(\frac{\Delta_A u}{U}\right)_{\max} = \frac{V\left(1 + 0{\cdot}4\beta\frac{d}{l}\right)}{4\pi B^3\beta^3}(K_A)_{\max} \quad .. \quad .. \quad .. \quad .. \quad .. \quad .. \quad (15)$$

The corresponding peak increments in velocity on the walls, if required for comparison with measured velocities, can be obtained by scaling up the peak blockage correction by a factor F, values of which have been plotted against Mach number, at constant values of $\bar{x}/B$, in Fig. 8. It should be noted that F varies considerably with Mach number and differs greatly from the convenient constant value given by the less precise doublet representation.

2.3. *Representation of a Wing.*—It can be shown, by an analysis similar to that of the preceding paragraph, that a wing in potential flow can be represented by a line source and equal line sink along the wing, the strength, δq, of which is given at any spanwise station by

$$2\bar{x}\,\delta q = US\left(1 + 1{\cdot}2\beta\,\frac{t}{c}\right)\delta y \qquad \ldots\ \ldots\ \ldots\ \ldots\ \ldots\ \ldots\ \ldots\ \ldots \quad (16)$$

where S is the local cross-sectional area and t/c the local thickness-ratio. The elements of source and sink are taken to be $\bar{x}$ forward and aft of the half-chord line.

If the origin of co-ordinate axes is taken at the mid-point of the half-chord line, equations (5) and (16) give the blockage at A $(x_0, 0, 0)$ as

$$\frac{\Delta_A u}{U} = \frac{1}{4\pi B^3\beta^3}\int_{-b}^{+b} \frac{\left(1 + 1{\cdot}2\beta\,\frac{t}{c}\right) S}{2\bar{x}} \left\{(x_0 - x' + \bar{x})\,K_A\left(\tfrac{x_0 - x' + \bar{x}}{\beta B},\ \tfrac{y'}{B},\ 0\right)\right.$$

$$\left. - (x_0 - x' - \bar{x})\,K_A\left(\tfrac{x_0 - x' - \bar{x}}{\beta B},\ \tfrac{y'}{B},\ 0\right)\right\} dy. \qquad \ldots\ \ldots\ \ldots\ \ldots\ \ldots\ \ldots \quad (17)$$

where x' is here the distance of the local half-chord point aft of the datum and $2b$ is the span of the wing.

For the purpose of evaluation of equation (17), it has been shown in Appendix B that any wing, unless of most unorthodox shape, can be represented by a non-tapered straight-swept wing of equal volume, mean angle of sweep and thickness ratio which has a span of $2\sqrt{3}\,k_1$, where k_1 is the radius of gyration of the original wing about the x-axis.

Values of $\bar{K}$ where

$$\bar{K} = \frac{1}{V}\int_{-b}^{+b} \frac{S}{2\bar{x}} \left\{(x_0 - x' + \bar{x})\,K\left(\tfrac{x_0 - x + \bar{x}}{\beta B},\ \tfrac{y}{B},\ 0\right) - (x_0 - x' - \bar{x})\,K\left(\tfrac{x_0 - x' - \bar{x}}{\beta B},\ \tfrac{y}{B},\ 0\right)\right\} dy \qquad (18)$$

and

$$\frac{\Delta u}{U} = \frac{V\left(1 + 1{\cdot}2\beta\,\frac{t}{c}\right)}{4\pi B^3\beta^3}\,\bar{K} \qquad \ldots\ \ldots\ \ldots\ \ldots\ \ldots\ \ldots\ \ldots\ \ldots\ \ldots \quad (19)$$

for non-tapered, straight-swept wings of spans from $0{\cdot}2B$ to $0{\cdot}6B$ and angles of sweep, φ, from $\tan^{-1}[(\tan\varphi)/\beta] = 0$ to 70 deg are plotted against $x_0/\beta B$ in Figs. 9 to 13, (a), (b) and (c). The centre-line blockage is given in Figs. (a) and side-wall and top and bottom-wall increments in velocity in Figs. (b) and (c) respectively. $\bar{K}$ is almost independent of $\bar{x}$ for the size of wing chord under consideration and a representative value for $\bar{x}$ of $0{\cdot}04B$ has been used.

Figs. 9 to 13 provide a ready means of estimating the longitudinal distribution of blockage and wall velocity increments for most wings. The peak values of $\bar{K}$ are given in a more compact form in Fig. 14, plotted against $\tan^{-1}[(\tan\varphi)/\beta]$ for constant values of $2\sqrt{3}\,k_1$.

Wings of delta plan-form are mostly of very small wing span relative to the tunnel, in which case they can be treated by the theory for bodies in section 2.2.

2.4. *Representation of a Wake.*—In general, the only known properties of the wake are those which can be derived from the measured drag, D, of the model. This information is sufficient to estimate the wake correction downstream of the model but the blockage and wall velocity increments over the model cannot be calculated without some assumption of the rate of dissipation of the wake. The usual practice is to represent the wake by a source on the axis of the tunnel at the position of the model. Although this cannot be justified theoretically, it appears to give fair agreement with experiment. The strength of the source is shown in Appendix C to be

$$q = 0{\cdot}7C_D SU, \qquad \ldots\ \ldots\ \ldots\ \ldots\ \ldots\ \ldots\ \ldots\ \ldots\ \ldots\ \ldots \quad (20)$$

where C_D is the drag coefficient (omitting induced drag) based on an area S.

In practice, the source is placed at approximately the centre of the model $(x', 0, 0)$. The increment in velocity at A $(x_o, 0, 0)$ due to the images of this source is given by equation (5) as

$$\frac{\delta_A u}{U} = \frac{0{\cdot}7C_D S}{4\pi B^2\beta^4}\left(\frac{x_0 - x'}{\beta B}\right) K_A\left(\tfrac{x_0 - x'}{\beta B}, 0, 0\right) \quad .. \quad .. \quad .. \quad .. \quad .. \quad (21)$$

which reaches a value far upstream of

$$\frac{[\delta_A u]_{-\infty}}{U} = \frac{0{\cdot}7C_D S}{4\pi B^2\beta^2}\left(-\frac{2\pi}{0{\cdot}7}\right) \quad .. \quad .. \quad .. \quad .. \quad .. \quad .. \quad .. \quad (22)$$

The uncorrected stream velocity is measured in terms of the wall pressures far upstream of the model, hence the blockage at $(x_0, 0, 0)$ is

$$\Delta_A u = \delta_A u - [\delta_A u]_{-\infty}$$

or

$$\frac{\Delta_A u}{U} = \frac{C_D S}{2B^2\beta^2}\left\{1 + \frac{0{\cdot}111(x_0 - x')}{\beta B} K_A\left(\tfrac{x_0 - x'}{\beta B}, 0, 0\right)\right\} \quad .. \quad .. \quad .. \quad .. \quad (23)$$

Similar expressions for the increments in velocity due to the wake on the side walls and top and bottom walls are obtained by replacing K_A by K_B and K_C respectively.

2.5. *Extension of the Theory to Speeds at Which Local Regions of Supersonic Flow are Present.*—The above theory has been developed on the assumption of subsonic potential flow. It can be extended to cover conditions where a supersonic region of limited extent exists at the model if the influence of the supersonic region on the induced velocity at a distant point be considered as roughly similar to that of a local bulge on the model surface. On this hypothesis, the formulae given above would remain applicable provided the volume term were increased by a factor dependent on the extent of the supersonic field.

A factor of this nature for the wing blockage formulae of section 2.3 has been derived empirically in section 6.2, making use of the measured increase in drag coefficient. Elongated three-dimensional bodies do not develop any considerable supersonic field at speeds within the present limit of subsonic tunnel tests and the formulae of section 2.2 can be used directly.

2.6. *Associated Changes in Pressure, Density, etc.*—The changes in velocity due to wall constraint must be associated with corresponding changes in other properties of the flow. These can readily be obtained from the equations of adiabatic flow at constant total-head. The two most often required are the change in local Mach number and the change in local $\frac{1}{2}\rho U^2$. If the ratio of specific heats, γ, is taken as $1{\cdot}4$, these are given by

$$\Delta M = M(1 + 0{\cdot}2M^2)\frac{\Delta u}{U} \quad .. \quad .. \quad .. \quad .. \quad .. \quad .. \quad .. \quad (24)$$

$$\frac{\Delta(\frac{1}{2}\rho U^2)}{\frac{1}{2}\rho U^2} = (2 - M^2)\frac{\Delta u}{U}$$

$$= \frac{(2 - M^2)}{M(1 + 0{\cdot}2M^2)}\Delta M \quad .. \quad .. \quad .. \quad .. \quad .. \quad .. \quad (25)$$

Tables of $(M/\beta^3)(1 + 0{\cdot}2M^2)$ and $(2 - M^2)/M(1 + 0{\cdot}2M^2)$ are given at the end of the text.

3. *Application of the Theory to the R.A.E. High Speed Wind Tunnel.*—In cross-section, the R.A.E. Subsonic Wind Tunnel is a 10×7 ft rectangle with flat-faced corner fillets (of face $2\sqrt{2}$ ft), as shown in Figs. 16 and 28. These fillets have been built over the original rounded corners as a means of improving the longitudinal velocity distribution. The cross-sectional area is now 62 sq ft in place of the 65 sq ft mentioned in Thom's paper[1].

The wall constraint formulae of section 2.2 and section 2.3 for a 10×7 rectangular wind tunnel can be modified to allow for these fillets by an overall correction as obtained in Appendix D. The centre-line blockage is found to be increased by $17\frac{1}{2}$ per cent, the side-wall increment by 12 per cent and the top and bottom-wall increment by $5\frac{1}{2}$ per cent.

The wake formulae of section 2.4 will be increased in inverse proportion to the change in area, *i.e.*, the velocity increment both at centre-line and walls will be increased by 13 per cent.

There is little knowledge of how the wall boundary layer upsets the above reflection theory. However, assuming reflection to occur at say $0{\cdot}3$ in $(0{\cdot}0025B)$ from the tunnel wall (where the velocity is about 70 per cent of stream velocity) the increments would be increased by only $1{\cdot}8$ per cent. The true increase, provided no break-away occurs due to the model, is probably smaller and has been neglected in the following work.

4. *Experimental Determination of Blockage.*—Although it is not possible to obtain a direct measurement of the velocity increment at the model due to blockage, there are a number of independent methods of checking the theoretical estimates. One is to compare force or pressure measurements on models of the same shape but of different sizes, the equivalent free-stream Mach number being obtained by extrapolation to an infinitely small model. In this way a mean blockage correction for each model is obtained. The measurements should preferably be made at the same Reynolds number. The method can only be used succesfully on models which show a rapid variation with Mach number of the coefficient measured. Also, a very high standard of accuracy of construction of the different models is required and it is difficult to make satisfactory allowance for interference of the supporting system.

An alternative and very much simpler procedure is to compare measured wall pressures with those given by the theory. It has been shown in section 2 that the velocity increments on the walls, which are due to the model and its images, are much greater than the blockage velocity increments at the model, which are due to the images only. Thus, although not an absolute check, the method gives a very useful indication of the reliability of the calculations. Static holes permanently set in the tunnel shell give an easy means of measuring the wall Mach numbers during any series of model tests.

5. *Experiments on Bodies of Revolution of Same Shape but Different Sizes.*—Five bodies have been mounted in turn in the R.A.E. wind tunnel on the end of a slender steel sting on the axis of the tunnel, and model drag and wall velocity increments measured over a range of Mach numbers up to tunnel choking. The overall dimensions of the bodies are given in Fig. 22 and a typical rig is shown in Fig. 23. Bodies 1 and 2 are of the same shape, fineness ratio 8 and of volume $0{\cdot}25$ and $0{\cdot}125$ ft^3 respectively. Bodies 3, 4 and 5 are also of similar shape, of fineness ratio 4 and of volume $0{\cdot}50$, $0{\cdot}25$ and $0{\cdot}125$ ft^3 respectively.

In these tests the Reynolds number was not constant, because of the resulting difficulty in obtaining accurate measurements, but this effect is not here considered serious. The Reynolds number per foot was constant at about $0{\cdot}5 \times 10^6$.

5.1. *Blockage Increments in Mach Number from Drag Measurements.*—Bodies 1 and 2 experienced little change in drag coefficient at Mach numbers up to $M = 0{\cdot}95$, but bodies 3, 4 and 5 showed a rapid rise above $M = 0{\cdot}9$. The measured rise in drag coefficient for each body is plotted in Fig. 24 against the measured (*i.e.*, uncorrected) Mach number, M_u. The broken line shows the extrapolated curve for a body of zero volume. The blockage correction to Mach number can be read off directly from horizontal intercepts between the curves, since the correction to $\frac{1}{2}\rho U^2$ has little effect. A comparison with the peak corrections calculated by the image theory, in which the body has been represented by an equivalent Rankine ovoid (equation (15) of section 2.2) and the wake by a source (equation (23) of section 2.4), is given in Fig. 26a. The full lines of Fig. 26 are obtained by using the calculated corrected Mach number in the compressibility factors and the broken lines by using the measured Mach number, M_u.

5.2. *Wall Increments in Mach Number.*—The experimental points for the peak increments in Mach number on the walls are given for bodies 1 and 2 in Fig. 25b and 25c and for bodies 3, 4 and 5 in Fig. 26b and 26c. Again the superimposed full lines are obtained by using the calculated corrected Mach number in the compressibility factors and the broken lines by using M_u. The agreement with the full lines is remarkably good and on this evidence the corrected Mach number is used in all further calculations.

The longitudinal distributions of ΔM on the side walls and on the top and bottom walls for bodies 1 and 3 at $M = 0{\cdot}94$ are given in Fig. 27. The agreement with the theoretical estimates shown is representative of that for all the bodies over the range of test Mach numbers.

6. *Experiments on Non-tapered Wings of Various Span and Sweepback.*—A series of non-tapered wings of symmetrical section, 1-ft chord, covering a range of aspect ratios $3{\cdot}6$, $3{\cdot}0$ and $2{\cdot}18$ and angle of sweep-back 0, 40 deg and 50 deg, have been tested up to choking Mach number, the models being supported by a small sting from the rear (Fig. 28). These tests were not primarily for investigations of blockage being part of a general research programme, but in all cases measurements were made of the increments in Mach number along the side walls of the tunnel.

6.1. *Wall Increments in Mach Number Due to the Wake.*—A typical measured longitudinal distribution of increment in Mach number on the side wall, $\Delta_B M$, due to a wing (unswept of span $0{\cdot}3B$) at $M_U = 0{\cdot}895$ is shown in Fig. 29. If the contribution from the wing is assumed to be symmetrical, and that from the wake to decrease and increase equally upstream and downstream respectively of the line of symmetry, it is possible, by taking differences in $\Delta_B M$, to obtain the distribution due to the wake only. This has been plotted at the foot of Fig. 29 and the calculated values from equation (23), in which K_A has been replaced by K_B, superimposed. The general good agreement for wake increments is shown in Fig. 30 in which all experimental values for the series have been plotted against the calculated values.

6.2. *Peak Wall Increments in Mach Number Due to the Wing.*—The contribution from the wing itself, also plotted in Fig. 29 for this typical case, is much larger than that given by the theory (equation 19). It was suggested in section 2.5 that such a discrepancy for wings at high Mach number might be attributed to the presence of a supersonic region near the model which acts as an increase in its effective size. In practice, spreading of the supersonic region is generally accompanied by an increase of drag, which suggests the possibility of obtaining an empirical correlation between the two. This is illustrated in Fig. 31, where the difference between measured and calculated peak wall incremental Mach numbers for the three unswept wings have been plotted against the product of the calculated wing contribution and ΔC_D, the rise in drag coefficient above the low-speed value. The results suggest increasing the source distribution strength by the factor $(1 + 14\Delta C_D)$, *i.e.*, incremental velocities due to a wing are given by

$$\frac{\Delta u}{U} = \frac{V(1 + 1{\cdot}2\beta\frac{t}{c} + 14\Delta C_D)}{4\pi B^3\beta^3}\bar{K} \qquad \ldots\ \ldots\ \ldots\ \ldots\ \ldots \quad (26)$$

where values of $\bar{K}$ are obtained from Figs. 9 to 13, (a), (b) and (c) for centre-line, side wall and top and bottom walls respectively at the appropriate span and angle of sweep.

7. *Experiments on Various Complete Models.*—Comparisons between the calculated and measured peak side wall increments in Mach number on a wide variety of models are given in Figs. 32a, 32b and 32c. Also a typical longitudinal distribution for a wing and body is given in Fig. 33. In each case the body has been represented by a source and sink, *i.e.*, a Rankine ovoid and the wing by a uniform line source and line sink of equivalent span swept back at the appropriate angle. The empirical factor $(1 + 14\Delta C_D)$ has been included for the wings and the compressibility factors are based on the corrected Mach number throughout. Corner fillets have been allowed for by use of the overall factors given in section 3.

Since the results show good agreement for wall velocity increments over a wide range of model configurations, the calculated values of centre-line blockage, which involve no greater assumptions, can be accepted with some confidence.

8. *Application.*—The formulae of section 2 are expressed in terms of the corrected Mach number and the drag coefficient, which is known initially at uncorrected Mach numbers only. Hence it is not possible to obtain a direct estimate of the blockage correction to be applied to a given tunnel measurement. The correction can be obtained either by a process of successive approximation or by graphical interpolation from tables of calculated values covering a range of corrected Mach numbers and drag coefficients. The latter method is preferable where a number of tests are made at various Mach numbers and incidences on the same model, a graph being prepared beforehand of correction against measured Mach number at constant values of C_D. A corresponding graph of peak side wall increments in Mach number can be used to obtain comparisons with observations during the test, thus providing a valuable check on the calculations.

It is essential to investigate the gradient in Mach number increment over the model at the higher Mach numbers of the tests. The lateral gradients, except for wings of very large span, are small, but for some configurations commonly tested, in particular a long body with a wing of small sweep, the longitudinal gradients can be large, the difference in Mach number increment for example between the wing and tailplane amounting to a third or more of the peak value. This condition, viewed in relation to the characteristics of the particular model, is usually the criterion which should determine the upper limit of the tests.

9. *Conclusions.*—It appears, from experience in the R.A.E. 10 × 7 ft Subsonic Wind Tunnel, that blockage corrections to measured velocity can be calculated, with sufficient accuracy for general purposes, by the method given in this paper. The model is replaced by a simple arrangement of sources and the constraining effect of the walls is represented by an infinite array of images of the sources in the walls of the tunnel, allowance for compressibility effects being made by the standard linear perturbation theory.

Use of a doublet in place of the model, in the manner of Refs. 1 and 2, is found to be too great an approximation. Instead, a body can be replaced by a single source and equal sink; a wing by a line of sources and line of sinks of appropriate strength and span and swept back at the appropriate angle. A wake is represented by a single source at the model.

It is shown experimentally that the corrected Mach number should be used in all compressibility factors. The method can be applied at Mach numbers up to 0·96, provided the correction does not exceed 3 or 4 per cent. An empirical factor, based on the measured rise in drag coefficient of the model, is used as a rough means of allowing for small supersonic regions of flow on a wing.

It is recommended that the validity of the blockage correction be examined in every doubtful case by calculation of the longitudinal distribution of the increment over the model and that a check of the accuracy be obtained by comparison of measured and calculated wall velocity increments.

A summary of the formulae required in practice is given in Appendix E.

REFERENCES

No.	*Author*	*Title, etc.*
1	Thom	Blockage Corrections in a Closed High Speed Wind Tunnel. R. & M. 2033. November, 9143.
2	Thompson	Present Methods of Applying Blockage Corrections in a Closed Rectangular High Speed Wind Tunnel. A.R.C. 11,385. January, 1948. (Unpublished.)
3	Allen and Vincenti	Wall Interference in a Two-dimensional Flow Wind Tunnel, with Consideration of the Effect of Compressibility. N.A.C.A. Report No. 782. 1944.

LIST OF SYMBOLS

B	Tunnel breadth
(x, y, z)	Co-ordinate axes defined in Fig. 1
U	Stream velocity
M_U	Measured stream Mach number
M	Corrected stream Mach number
$\beta = \sqrt{(1 - M^2)}$	; except as used in Appendix C
Φ	Velocity potential
δq_1	Volume flow due to a source in incompressible flow
$\delta q, q$	Volume flow due to a source in compressible flow
$r = \sqrt{(y^2 + z^2)}$	
$\Delta_A u$	Velocity increment at $(x_0, 0, 0)$ on centre-line of tunnel due to wall constraint (blockage correction)
$\Delta_B u$	Velocity increment at $(x_0, 0{\cdot}5B, 0)$ on side wall (width $0{\cdot}7B$) of tunnel
$\Delta_C u$	Velocity increment at $(x_0, 0, 0{\cdot}35B)$ on top and bottom wall (width B)
K_A	Defined in equation (5) and Fig. 2
K_B	Defined in equation (7) and Fig. 3
K_C	Defined in equation (9) and Fig. 4
V	Volume of body or wing
A	Cross-sectional area of body
d	Maximum diameter of body
l	Length of body
$(x', y', 0)$	Location of centre of volume of body or of local half-chord point of wing
$\bar{x}$	Distance of equivalent source and sink from centre of volume of body or half-chord of wing
k_2	Minimum radius of gyration of body in pitch
$(K_A)_{\max} = K_A$	at $\left(\frac{\bar{x}}{\beta B}, 0, 0\right)$
F	Ratio of wall increment in velocity to tunnel centre-line increment
S	Local cross-sectional area of wing
t	Local maximum thickness of wing
c	Local chord of wing
b	Semi-span of wing
k_1	Minimum radius of gyration of wing in roll
φ	Angle of sweepback of half-chord line of wing
$\bar{K}$	Defined in equation (18)
ρ	Density
C_D	Drag coefficient, omitting induced drag
ΔC_D	Rise in drag coefficient above low speed value
C	Tunnel cross-sectional area
γ	Ratio of specific heats

APPENDIX A

Representation of a Body by the Best Rankine Ovoid

The blockage increment in velocity, $\Delta_A u$, at $(x_0, 0, 0)$ due to a body on the axis of the tunnel is given by equation (11) as

$$\frac{\Delta_A u}{U} = \frac{\left(1 + 0{\cdot}4\beta\frac{d}{l}\right)}{4\pi B^3\beta^3}\int (x_0 - x)\frac{dA}{dx} K_{A\left(\frac{x_0 - x}{\beta B},\, 0,\, 0\right)}\, dx \qquad .. \quad .. \quad .. \quad .. \quad (26)$$

where

$$K_{A\left(\frac{x}{\beta B},\, 0,\, 0\right)} = \sum_{m=-\infty}^{\infty}\sum_{n=-\infty}^{\infty}\left\{\left(\frac{x}{\beta B}\right)^2 + m^2 + 0{\cdot}49\, n^2\right\}^{-3/2}$$

omitting the term $m = n = 0$ . .. . (27)

The corresponding expression for $\Delta_A u$ due to a Rankine ovoid formed by a source at $(x' - \bar{x}, 0,0)$ and a sink at $(x' + \bar{x}, 0, 0)$ is given by equation (13) as

$$\frac{\Delta_A u}{U} = \frac{\left(1 + 0{\cdot}4\beta\frac{d}{l}\right)}{4\pi B^3\beta^3}\int \frac{(x_0 - x)}{2\bar{x}}\frac{dA}{dx}\left\{(x_0 - x' + \bar{x})\, K_{A\left(\frac{x_0 - x' + \bar{x}}{\beta B},\, 0,\, 0\right)}\right.$$

$$\left. - (x_0 - x' - \bar{x})\, K_{A\left(\frac{x_0 - x' - \bar{x}}{\beta B},\, 0,\, 0\right)}\right\} dx \qquad .. \quad .. \quad .. \quad .. \quad .. \quad (28)$$

since $$V = \int (x_0 - x)\frac{dA}{dx}\, dx\,.$$

Thus to represent the body by a Rankine ovoid for the purpose of calculating blockage we must choose x' and $\bar{x}$ to give the best general approximation to

$$\int (x_0 - x)\frac{dx}{dA}\left\{K_{A\left(\frac{x_0 - x}{\beta B}\right)} - \frac{(x_0 - x' + \bar{x})}{2\bar{x}} K_{A\left(\frac{x_0 - x' + \bar{x}}{\beta B}\right)} + \frac{(x_0 - x' - \bar{x})}{2\bar{x}} K_{A\left(\frac{x_0 - x' - \bar{x}}{\beta B}\right)}\right\} dx = 0 \quad .. \quad (29)$$

Expanding equation (27), (for $(x^2/\beta^2 B^2) < m^2 + 0{\cdot}49\, n^2$),

$$K_{A\left(\frac{x}{\beta B},\, 0,\, 0\right)} = \Sigma\ \Sigma\ (m^2 + 0{\cdot}49n^2)^{-3/2}\left\{1 - \frac{3}{2}\frac{x^2}{\beta^2 B^2 (m^2 + 0{\cdot}49\, n^2)}\right.$$

$$\left. + \frac{15}{8}\frac{x^4}{\beta^4 B^4 (m^2 + 0{\cdot}49n^2)^2} + \ldots\ldots\ldots\right\}$$

Thus, over most of the field, it is possible to satisfy the first two terms in the expansion of equation (29) by making

$$\int \frac{(x_0 - x)}{2\bar{x}} \frac{dA}{dx} \left\{ (x_0 - x)^2 2\bar{x} - (x_0 - x' + \bar{x})^3 + (x_0 - x' - \bar{x})^3 \right\} dx = 0$$

which can be rearranged as

$$\int \frac{dA}{dx} \left\{ - (x - x')^3 + 3(x_0 - x')(x - x')^2 + \bar{x}^2(x - x') - (x_0 - x')[2(x_0 - x')^2 - \bar{x}^2] \right\} dx = 0$$

Hence, if the centre of the Rankine ovoid is taken at the centre of volume of the body, *i.e.*,

$$\int \frac{dA}{dx} (x - x')^2 dx = 0$$

we have

$$\bar{x}^2 = \frac{\int (x - x')^3 \frac{dA}{dx} dx}{\int (x - x') \frac{dA}{dx} dx} = 3k_2^2 \quad \ldots \quad \ldots \quad \ldots \quad \ldots \quad \ldots \quad \ldots \quad (31)$$

where, for a slender body, k_2 is the radius of gyration about an axis through the centre of volume in the plane $x = 0$. The success of this approximation is illustrated in Figs. 5 and 6.

Thus the blockage incremental velocities are approximately those due to a source and equal sink, of strength $(V/2\sqrt{3}k_2)$, at a distance $\pm \sqrt{3}k_2$ from the centre of volume of the body, where k_2 is the minimum radius of gyration in a plane normal to the stream.

APPENDIX B

Representation of a Wing by a Uniform Line Source and Line Sink of Appropriate Span

From section 2.3, any wing in potential flow can be represented for the purpose of calculating induced velocities at some distance from the wing, by a line source and line sink along the wing the strength at any point of which is proportional to the local cross-sectional area, S. The blockage incremental velocity, $\Delta_A u$, at the origin, which is taken at the mid-point of the half-chord line, is given by equation (17) as

$$\frac{\Delta_A u}{U} = \frac{\left(1 + 1{\cdot}2\beta\frac{t}{c}\right)}{4\pi B^3\beta^3}\int_{-b}^{b}\frac{S}{2\bar{x}}\left\{(-y\tan\varphi + \bar{x})K_A\left(\frac{-y\tan\varphi+\bar{x}}{\beta B}, \frac{y}{B}, 0\right)\right.$$

$$\left. - (-y\tan\varphi - \bar{x})K_A\left(\frac{-y\tan\varphi-\bar{x}}{\beta B}, \frac{y}{B}, 0\right)\right\} dy \quad .. \quad .. \quad .. \quad .. \quad .. \quad .. \quad (32)$$

where φ is the mean angle of sweep and t/c the mean thickness ratio.

Now,

$$K_A\left(\frac{-y\tan\varphi+\bar{x}}{\beta B}, \frac{y}{B}, 0\right) = \sum_{m=-\infty}^{\infty}\sum_{n=-\infty}^{\infty}\left\{\left(\frac{-y\tan\varphi+\bar{x}}{\beta B}\right)^2 + \left(m + (-1)^m\frac{y}{B}\right)^2 + 0{\cdot}49n^2\right\}^{-3/2}$$

omitting the term $m = n = 0$

$$= \Sigma\Sigma\left\{\frac{1}{(m^2+0{\cdot}49n^2)^{3/2}} - \frac{3}{2}\frac{\left[\left(1+\frac{\tan^2\varphi}{\beta^2}\frac{y^2}{B^2}\right) - 2\bar{x}\frac{\tan\varphi}{\beta^2 B^2}y + 2(-1)^m m\frac{y}{B} + \frac{\bar{x}^2}{\beta^2B^2}\right]}{(m^2+0{\cdot}49n^2)^{5/2}} + \ldots.\right\} \quad (33)$$

Considering the major terms only in this expansion, equation (32) becomes

$$\frac{\Delta_A u}{U} = \frac{\left(1+1{\cdot}2\beta\frac{t}{c}\right)}{4\pi B^3\beta^3}\Sigma\Sigma\left\{\frac{1}{(m^2+0{\cdot}49n^2)^{3/2}}\int_{-b}^{b}S\,dy - \frac{3}{2(m^2+0{\cdot}49n^2)^{5/2}}\int_{-b}^{b}S\left[1+\frac{2\tan^2\varphi}{\beta^2}\right]\frac{y^2}{B^2}dy\right\}$$

$$= \frac{V\left(1+1{\cdot}2\beta\frac{t}{c}\right)}{4\pi B^3\beta^3}\Sigma\Sigma\left\{\frac{1}{(m^2+0{\cdot}49n^2)^{3/2}} - \frac{3}{2(m^2+0{\cdot}49n^2)^{5/2}}\left[1+\frac{2\tan^2\varphi}{\beta^2}\right]k_1^2\right\} \quad .. \quad (34)$$

where for a thin wing k_1 is the radius of gyration about the x-axis. The analysis also applies to any point $(x_0, 0, 0)$ on the axis.

It follows that, for the purpose of calculating blockage, any wing can be represented approximately by a non-tapered wing of equal volume, mean angle of sweep and thickness ratio which has a span of $2\sqrt{3}k_1$, where k_1 is the radius of gyration of the original wing about the roll axis.

The centre-line and side wall K terms for two wings, of taper-ratio 3 : 1 and sweepback of 0 and 60 deg respectively, are compared in Fig. 15 with those of the equivalent non-tapered wings.

APPENDIX C

Wake Blockage in any Closed Wind Tunnel

Consider a station at a short distance downstream of the model where the static pressure has regained a constant value across the tunnel. Let αU, $\beta\rho$, $p + \Delta p$ be the velocity, density and pressure in any element, δC, of the wake at this station and $U + \Delta U$, $\rho + \Delta\rho$, $p + \Delta p$ be the velocity, density and pressure outside the wake. U, ρ, p are the corresponding values in the undisturbed flow upstream of the model and C is the cross-sectional area of the tunnel.

The stream outside the wake is isentropic and we have

$$\frac{\Delta U}{U} = -\frac{p}{\rho U^2}\frac{\Delta p}{p} = -\frac{\gamma p}{\rho U^2}\frac{\Delta\rho}{\rho} . \qquad \ldots\ldots\ldots\ldots\ldots (35)$$

The continuity equation is

$$\rho UC = (\rho + \Delta\rho)\,(U + \Delta U)\,(C - \int \delta C) + \int \alpha\beta\rho U\,\delta C$$

or

$$\frac{\Delta\rho}{\rho} + \frac{\Delta U}{U} = \int (1 - \alpha\beta)\frac{\delta C}{C} \qquad \ldots\ldots\ldots\ldots\ldots\ldots (36)$$

where the integral is taken across the wake.

Also, if D is the drag of the model, the momentum equation is

$$(p + \Delta p)C + (\rho + \Delta\rho)(U + \Delta U)^2\,(C - \int \delta C) + \int \alpha^2\beta\rho U^2\,\delta C - (p + \rho U^2)C = -D$$

or

$$-\frac{p}{\rho U^2}\frac{\Delta p}{p} - \frac{\Delta\rho}{\rho} - 2\frac{\Delta U}{U} = \frac{D}{\rho U^2 C} - \int (1 - \alpha^2\beta)\frac{\delta C}{C} \qquad \ldots\ldots\ldots (37)$$

Writing $\dfrac{\rho U^2}{\gamma p} = M^2$, equations (35) and (36) give

$$(1 - M^2)\frac{\Delta U}{U} = \int (1 - \alpha\beta)\frac{\delta C}{C}$$

and equations (35) and (37) give

$$(1 - M^2)\frac{\Delta U}{U} = -\frac{D}{\rho U^2 C} + \int (1 - \alpha^2\beta)\frac{\delta C}{C} .$$

Hence,

$$\frac{\Delta U}{U} = \frac{D}{\rho U^2 C(1 - M^2)}\frac{\int (1 - \alpha\beta)\frac{\delta C}{C}}{\int \alpha\beta(1 - \alpha)\frac{\delta C}{C}} . \qquad \ldots\ldots\ldots\ldots (38)$$

In incompressible flow, $\beta = 1$ and

$$\left(\frac{\Delta U}{U}\right)_i = \frac{D}{\rho U^2 C}\frac{\int (1 - \alpha)\frac{\delta C}{C}}{\int \alpha\,(1 - \alpha)\frac{\delta C}{C}} .$$

The form of velocity distribution in the wake has little influence on $\Delta U/U$ and it is sufficiently accurate to assume a constant mean value of α, which we shall term $\bar{\alpha}$, *i.e.*,

$$\left(\frac{\Delta U}{U}\right)_i = \frac{D}{\rho U^2 C \bar{\alpha}} \quad .. \quad .. \quad .. \quad .. \quad .. \quad .. \quad .. \quad .. \quad (39)$$

where $\bar{\alpha}$ increases from a value of about 0·9 just downstream of the model to near unity far downstream.*

A similar simplification of the general formula (38) gives

$$\frac{\Delta U}{U} = \frac{D}{\rho U^2 C(1 - M^2)} \frac{1 - \bar{\alpha}\,\bar{\beta}}{\bar{\alpha}\bar{\beta}(1 - \bar{\alpha})} \cdot \quad .. \quad .. \quad .. \quad .. \quad .. \quad (40)$$

If transfer of heat to the model can be neglected, the energy equation, to the accuracy required here, is

$$\frac{U^2}{2} + \frac{\gamma}{\gamma - 1}\frac{p}{\rho} = \bar{\alpha}^2 \frac{U^2}{2} + \frac{\gamma}{\gamma - 1}\frac{p}{\beta\rho} \quad .. \quad .. \quad .. \quad .. \quad .. \quad .. \quad (41)$$

i.e., $$(1 - \bar{\alpha}^2)\frac{\gamma - 1}{2} M^2 = \frac{1}{\bar{\beta}} - 1$$

from which $$\frac{1 - \bar{\alpha}\bar{\beta}}{\bar{\beta}(1 - \bar{\alpha})} = 1 + \frac{\frac{1}{\bar{\beta}} - 1}{1 - \bar{\alpha}} = 1 + \frac{1 + \bar{\alpha}}{2}(\gamma - 1) M^2. \quad .. \quad .. \quad .. \quad (42)$$

Combining equations (40) and (42),

$$\frac{\Delta U}{U} = \frac{D}{\rho U^2 C(1 - M^2)} \frac{1}{\bar{\alpha}} \left\{1 + \frac{1 + \bar{\alpha}}{2}(\gamma - 1) M^2\right\}. \quad .. \quad .. \quad .. \quad (43)$$

The velocity increment, ΔU, and the associated pressure and density changes of equation (35) would not be present in an unbounded stream (C infinitely large) and, consequently, are a measure of the blockage increments due to the wake.

---

* A cosine distribution of $1 - \alpha$ would give

$$\left(\frac{\Delta U}{U}\right) = \frac{D}{\rho U^2 C}(1 - \bar{\alpha})\frac{\pi}{2}\int_{-\pi/2}^{\pi/2} \cos\theta\, d\theta \Big/ (1 - \bar{\alpha})\frac{\pi}{2}\int_{-\pi/2}^{\pi/2} \cos\theta \left\{1 - (1 - \bar{\alpha})\frac{\pi}{2}\cos\theta\right\} d\theta$$

$$= \frac{D}{\rho U^2 C} \frac{1}{1 - \frac{\pi^2}{8}(1 - \bar{\alpha})}$$

$$= 1{\cdot}14 \frac{D}{\rho U^2 C} \text{ at } \bar{\alpha} = 0{\cdot}9$$

whereas the simpler equation (39) gives

$$\left(\frac{\Delta U}{U}\right)_i = 1{\cdot}11 \frac{D}{\rho U^2 C} \text{ at } \bar{\alpha} = 0{\cdot}9$$

In general, the value of $\bar{a}$ at short distances downstream of the model is of the order of $0{\cdot}9$. Thus the factor $\frac{1}{\bar{a}}\left\{1+\frac{1+\bar{a}}{2}(\gamma-1)M^2\right\}$ has a low speed value of the order of $1{\cdot}1$ which increases to the order of $1{\cdot}5$ at $M=0{\cdot}95$. The wake blockage is usually important only at high subsonic Mach numbers, so, failing more exact information on the wake, it is convenient to replace $\frac{1}{\bar{a}}\left\{1+\frac{1+\bar{a}}{2}(\gamma-1)M^2\right\}$ by a constant factor of $1{\cdot}4$ (value for $\bar{a}=0{\cdot}9$, $M=0{\cdot}85$), *i.e.*,

$$\left(\frac{\Delta U}{U}\right)_{\max}=1{\cdot}4\frac{D}{\rho U^2C(1-M^2)}. \qquad \ldots\ldots\ldots\ldots\ldots\ldots \quad (44)$$

An estimation of the correction in the neighbourhood of the model requires some assumption of the rate of dissipation of the wake. A simple procedure, which cannot be justified theoretically, but which appears to give fair agreement with experiment, *e.g.*, Fig. 29, is to represent the wake by a source on the axis of the tunnel at the position of the model. The source strength is chosen so that, for the same upstream conditions, the increment in velocity downstream of the source is equal to the maximum value due to the model.

If q is the volume flow of the source and $U+\delta U$, $\rho+\delta\rho$, $p+\delta p$ the velocity, density and pressure downstream of the source, the continuity equation is

$$(\rho+\delta\rho)(U+\delta U)C-\rho UC=q\,.$$

Since the flow is isentropic,

$$\frac{\delta U}{U}=-M^2\frac{\delta\rho}{\rho}$$

giving

$$\frac{\delta U}{U}=\frac{q}{UC(1-M^2)} \qquad \ldots\ldots\ldots\ldots\ldots\ldots \quad (45)$$

and the strength of the representative source, from equations (44) and (45) as

$$q=\frac{1{\cdot}4\,D}{\rho UC}$$

$$=0{\cdot}7C_DSU \qquad \ldots\ldots\ldots\ldots\ldots\ldots \quad (46)$$

where C_D is the drag coefficient based on an area S.

This value of source strength is slightly larger than the value

$$q=\tfrac{1}{2}C_DSU\{1+(\gamma-1)M^2\}$$

obtained by Allen and Vincenti[3], and the value

$$q=\tfrac{1}{2}C_DSU$$

obtained by Thom[1].

APPENDIX D

Effect of Corner Fillets in a 10×7 *ft Rectangular Wind Tunnel*

The R.A.E. High Speed Wind Tunnel has a 10 by 7 ft rectangular working-section with flat-faced corner fillets of face $2\sqrt{2}$ ft (*see* Fig. 16a). In order to calculate the constraining effect of these fillets in addition to that of the rectangular tunnel ($B \times 0{\cdot}7B$) considered in section 2, it is convenient to consider the section as a square, of side $b = (1{\cdot}3/\sqrt{2})B$, having two large fillets, of face $0{\cdot}6B$, and two smaller fillets of face $0{\cdot}3B$ (Fig. 16b).

Fig. 17 gives the longitudinal distribution of velocity along an axis C (defined in Fig. 16), in a direction normal to the face FG, induced by a doublet, μ, on the centre-line, A, of the square tunnel and its images in the walls of the tunnel. This normal velocity can be made zero (representing the condition with fillets) by a suitable arrangement of sources and sinks along the corner axis, D. The longitudinal distribution of normal velocity along C due to a single source on D and its images in the square tunnel is given in Fig. 18. From this data, it is possible, by solution of a set of simultaneous equations, to determine the strengths of any given number of sources arbitrarily placed along D which will make the normal velocity exactly zero at an equal number of points arbitrarily chosen along C. In practice, five sources so determined make the normal velocity sufficiently small at all points along C.

Distance upstream of model	*Strength of source on axis D*
$0{\cdot}1b$	$1{\cdot}540 \times 3/\sqrt{2}.\mu/b$
$0{\cdot}2b$	$-0{\cdot}090$,,
$0{\cdot}3b$	$0{\cdot}099$,,
$0{\cdot}5b$	$-0{\cdot}014$,,
$0{\cdot}8b$	$-0{\cdot}010$,,

There will be a corresponding set of sources and sinks of opposite sign on the downstream side of the model.

The sources and sinks represent a fillet which touches the desired flat-faced fillet along the axis C but which is slightly more convex near the model and slightly more concave some distance upstream of the model. Investigation of the normal velocity along an axis J, midway between C and the edge of the fillet (using data given in Figs. 17 and 18) has indicated the boundary to be always within $0{\cdot}003B$ of J.

In a similar manner sources arranged along the corner axis E can be found to represent the smaller fillets by inducing an equal and opposite normal velocity at B to that induced by the doublet and its images and the sources along D and their images.

Distance upstream of model	*Strength of source on axis E*
$0{\cdot}1b$	$0{\cdot}030 \times 3/\sqrt{2}.\mu/b$
$0{\cdot}2b$	0 ,,
$0{\cdot}3b$	$0{\cdot}039$,,
$0{\cdot}4b$	$0{\cdot}018$
$0{\cdot}5b$	$0{\cdot}003$

The effect of the sources along E on the velocities at the larger fillet is negligible.

The longitudinal induced velocities at A, B, and C due to the doublet and its images and to a source at any point along D and E and its images are given in Figs. 19 and 20. We then have, by summation, the blockage correction at points along the axis of the tunnel, and the velocity increments along the tunnel walls (on the side wall at B and the top and bottom walls at C, shown

in Fig. 21. The values of centre-line blockage obtained in section 2 for a rectangular wind tunnel, increased by $17\frac{1}{2}$ per cent, and the corresponding values for the walls, increased by 12 per cent and $5\frac{1}{2}$ per cent respectively have been superimposed on Fig. 21. The agreement suggests that overall corrections of this order can be applied to estimates from section 2 as a means of allowing for the corner fillets.

It is of interest to compare the above values with those for wind-tunnels of other shape by expressing the peak increment in velocity in the form

$$\Delta u = \frac{\mu G}{C^{3/2}}$$

where C is the cross-sectional area of the tunnel. Values of G and of F, the ratio of peak wall increment to blockage increment, for a doublet are as follows,

	G	F	
		smaller wall	*larger wall*
Circular wind tunnel	0·708	2·22	
Square wind tunnel	0·723	2·59	2·59
10 × 7 ft wind tunnel with corner fillets	0·749	1·73	3·19
10 × 7 rectangular wind tunnel	0·766	1·81	3·56
2 × 1 rectangular wind tunnel	0·914		

The method of allowing for corner fillets suggested in Ref. 1, which was to increase all increments in proportion to $C^{3/2}$ (*i.e.*, keeping G constant at 0·766), gives, in the above case, a numerical correction of 20 per cent.

APPENDIX E

Summary of 'Blockage' Formulae

Rectangular wind-tunnel $B \times 0{\cdot}7B$.

Co-ordinate axes defined in Fig. 1.

$\Delta_A M$ Increment in Mach number at $(x_0, 0, 0)$ on the centre-line of the tunnel due to wall constraint (blockage correction).

$\Delta_B M$ Increment in Mach number at $(x_0, 0{\cdot}5B, 0)$ on the centre-line of the side wall (width $0{\cdot}7B$) due to model.

$\Delta_C M$ Increment in Mach number at $(x_0, 0, 0{\cdot}35B)$ on the centre-line of the top and bottom walls (width $1{\cdot}0B$) due to model.

The corrected Mach number must be used in all compressibility factors. For this reason, it is usually simpler to select values of corrected Mach number and obtain the corresponding drag coefficients by trial and error. The required increments at any measured Mach number can then be obtained by interpolation.

Increments due to various components of the model and to the wake are added at the same corrected Mach number to give the total blockage correction and wall increments, at any point.

Bodies

Centre of volume at $(x', y', 0)$,

$$\Delta M = \frac{M}{\beta^3}(1 + 0{\cdot}2M^2)\left(1 + 0{\cdot}4\beta\frac{d}{l}\right)\frac{V}{4\pi B^3}$$

$$\left\{\frac{\dfrac{(x_0 - x' + \bar{x})}{\beta B} K_{\left(\frac{x_0 - x' - \bar{x}}{\beta B}, \frac{y'}{B}, 0\right)} - \dfrac{(x_0 - x' - \bar{x})}{\beta B} K_{\left(\frac{x_0 - x' - \bar{x}}{\beta B}, \frac{y'}{B}, 0\right)}}{\dfrac{2\bar{x}}{\beta B}}\right\}$$

where V = volume,

l/d = fineness-ratio,

$\bar{x} = \sqrt{3}k_2$, where k_2 is the radius of gyration about an axis through the centre of volume normal to the stream,

$\dfrac{x}{\beta B} K_{\left(\frac{x}{\beta B}, \frac{y}{B}, 0\right)}$ is given in Figs. 2, 3 and 4,

β, $\dfrac{1}{\beta}$ and $\dfrac{M}{\beta^3}(1 + 0{\cdot}2M^2)$ are given in Table 1.

Alternatively, peak increments are given by

$$(\Delta_A M)_{\max} = \frac{M}{\beta^3}(1 + 0{\cdot}2M^2)\left(1 + 0{\cdot}4\beta\frac{d}{l}\right)\frac{V}{4\pi B^3}(K_A)_{\max},$$

$$(\Delta_B M)_{\max} = F_B(\Delta_A M)_{\max},$$

$$(\Delta_C M)_{\max} = F_C(\Delta_A M)_{\max},$$

where $(K_A)_{\max}$ is given against Mach number at constant $\bar{x}/B$ in Fig. 7, and F is given against Mach number at constant $\bar{x}/B$ in Fig. 8.

(52308) B 2

Wings

Mid-point of half-chord line at origin.

$$\Delta M = \frac{M}{\beta^3}\,(1 + 0{\cdot}2M^2)\left(1 + 1{\cdot}2\beta\,\frac{t}{c} + 14\Delta C_D\right)\frac{V}{4\pi B^3}\,\bar{K}$$

where

V	volume,
t/c	mean thickness ratio,
φ	mean angle of sweep,
k_1	radius of gyration about roll axis,
ΔC_D	rise in drag coefficient of model (based on wing area) above low speed value,

$\bar{K}$ is given against $x_0/\beta B$ at constant values of $\varphi_M = \tan^{-1}\left\{\frac{1}{\beta}\tan\varphi\right\}$ and $2\sqrt{3}\,k_1/B$ in Figs. 9 to 13,

β, $\frac{1}{\beta}$ and $\frac{M}{\beta^3}\,(1 + 0{\cdot}2M^2)$ are given in Table 1.

Alternatively, peak increments are given by

$$(\Delta M_{\max} = \frac{M}{\beta^3}\,(1 + 0{\cdot}2M^2)\left(1 + 1{\cdot}2\beta\,\frac{t}{c} + 14\Delta C_D\right)\frac{V}{4\pi B^3}\,(\bar{K})_{\max},$$

where $(\bar{K})_{\max}$ is given against φ_M at constant values of $2\sqrt{3}\,k_1/B$ in Fig. 14.

Note: Wings of small span and high taper (*e.g.*, Delta wings) are best treated as bodies.

Wakes

Centre of model at $(x', 0, 0)$,

$$\Delta M = \frac{M}{\beta_2}\,(1 + 0{\cdot}2M^2)\,\frac{C_D S}{2B^2}\left\{1 + 0{\cdot}111\,\frac{(x_0 - x')}{\beta B}\,K_{\left(\frac{x_0 - x'}{\beta B},\,0,\,0\right)}\right\}$$

where C_D is the drag coefficient of model, omitting induced drag, based on an area S,

$\frac{x}{\beta B}\,K_{\left(\frac{x}{\beta B},\,0,\,0\right)}$ is given in Figs. 2, 3 and 4.

$\beta, \frac{1}{\beta}, \frac{M}{\beta^3}\,(1 + 0{\cdot}2M^2)$ are given in Table 1.

Application to the R.A.E. Wind Tunnel.—In applying the above formulae to the R.A.E. 10 × 7 ft Wind Tunnel with the present shape of corner fillets (Fig. 16a) we have,
for bodies or wings,

$$\Delta_A M = 1{\cdot}175 \times (\Delta_A M \text{ calculated by above formulae using } B = 10 \text{ ft})$$
$$\Delta_B M = 1{\cdot}12 \times (\Delta_B M \text{ calculated by above formulae using } B = 10 \text{ ft})$$
$$\Delta_C M = 1{\cdot}055 \times (\Delta_C M \text{ calculated by above formulae using } B = 10 \text{ ft})$$

for wakes,

$$\Delta M = 1{\cdot}13 \times (\Delta M \text{ calculated by above formulae using } B = 10 \text{ ft}).$$

TABLE 1

M	β	$\frac{1}{\beta}$	$\frac{M(1+\frac{1}{5}M^2)}{\beta^3}$	$\frac{(2-M^2)}{M(1+\frac{1}{5}M^2)}$
0·20	0·9798	1·0206	0·2143	9·7222
0·30	0·9539	1·0483	0·3518	6·2541
0·40	0·9165	1·0911	0·5362	4·4574
0·50	0·8660	1·1547	0·8083	3·3333
0·60	0·8000	1·2500	1·2562	2·5498
0·64	0·7684	1·3015	1·5263	2·2969
0·68	0·7332	1·3639	1·8847	2·0697
0·70	0·7141	1·4003	2·1103	1·9646
0·72	0·6940	1·4410	2·3778	1·8644
0·74	0·6726	1·4868	2·6981	1·7691
0·76	0·6499	1·5387	3·0882	1·6778
0·78	0·6258	1·5980	3·5701	1·5906
0·80	0·6000	1·6667	4·1778	1·5071
0·82	0·5724	1·7471	4·9613	1·4271
0·84	0·5426	1·8430	6·0004	1·3504
0·86	0·5103	1·9597	7·4293	1·2767
0·88	0·4750	2·1054	9·4848	1·2059
0·90	0·4359	2·2942	12·6274	1·1379
0·92	0·3919	2·5515	17·8688	1·0724
0·94	0·3412	2·9311	27·8530	1·0093
0·96	0·2800	3·5714	51·7903	0·9485

$$\Delta_A u = \frac{\delta q\,(x_0 - x)}{4\pi\,\beta^3 B^3} K_A$$

WHERE $K_A = \sum_{m=-\infty}^{\infty} \sum_{n=-\infty}^{\infty} \left\{ \left(\frac{x_0 - x}{\beta B}\right)^2 + \left(m + (-1)^m \frac{y}{B}\right)^2 + (0{\cdot}7n)^2 \right\}^{-3/2}$

OMITTING THE TERM $m = n = 0$

(CO-ORDINATE AXES DEFINED IN FIG. 1)

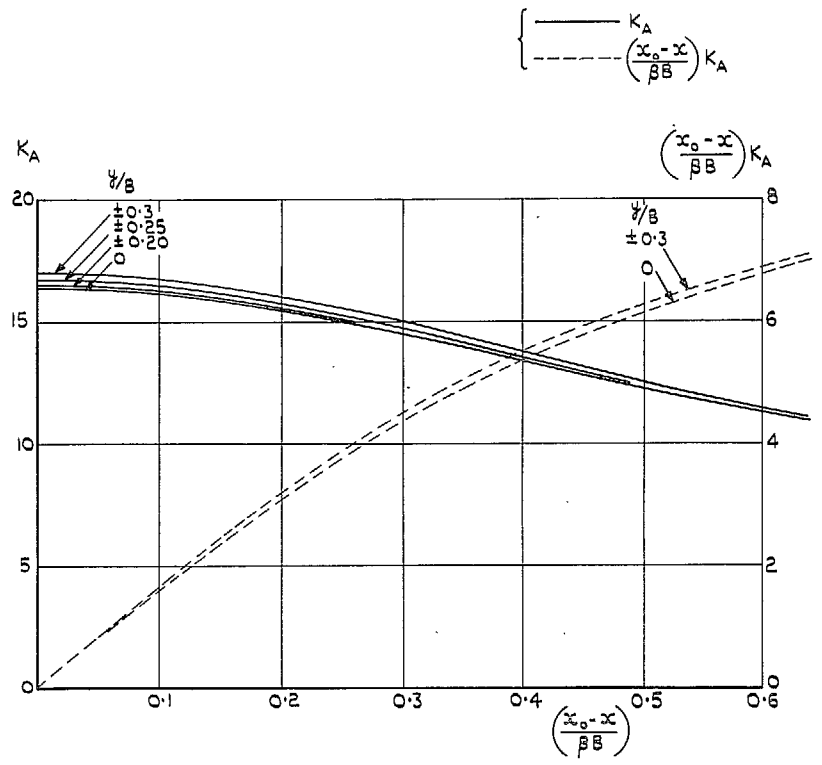

FIG. 2. Increment in velocity, $\Delta_A u$, at $(x_0, 0, 0)$ on the centre line due to the images of a source, δq, at $(x, y, 0)$ in a rectangular tunnel $(B \times 0{\cdot}7B)$.

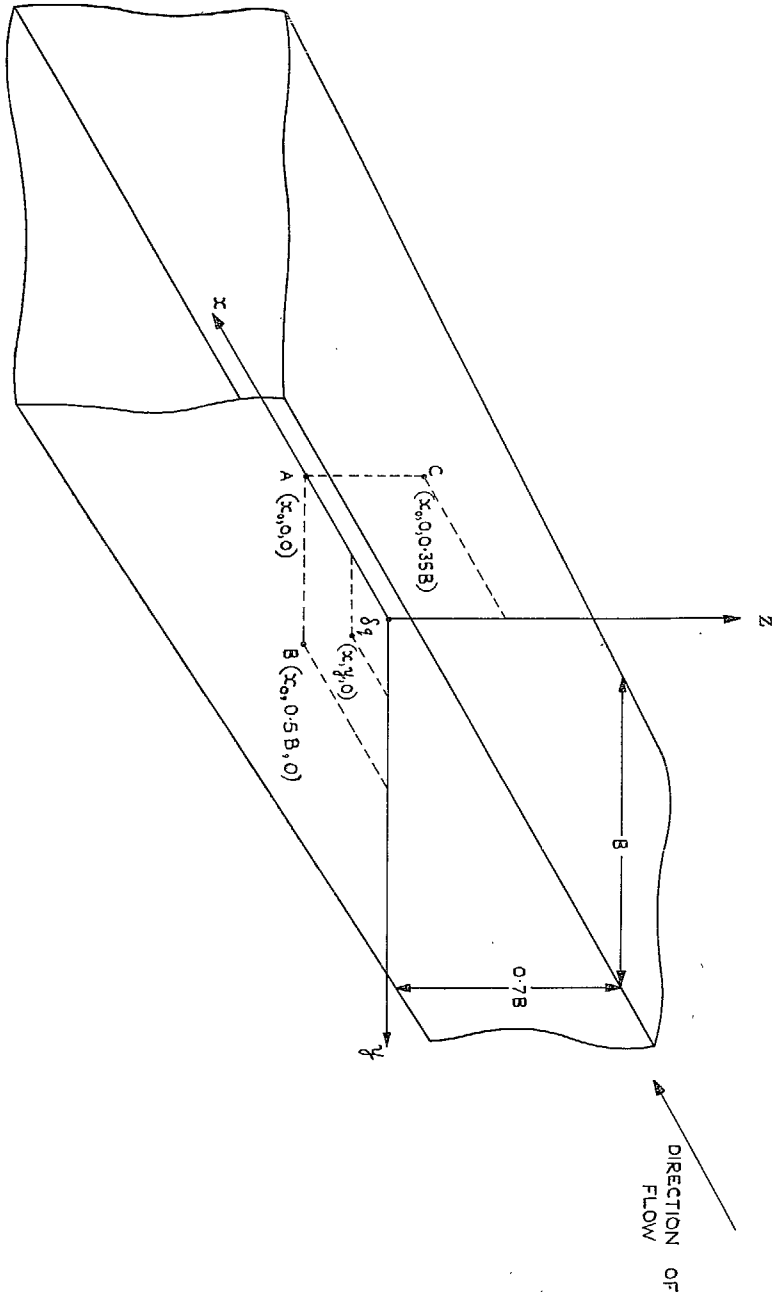

FIG. 1. Co-ordinate axes of reference.

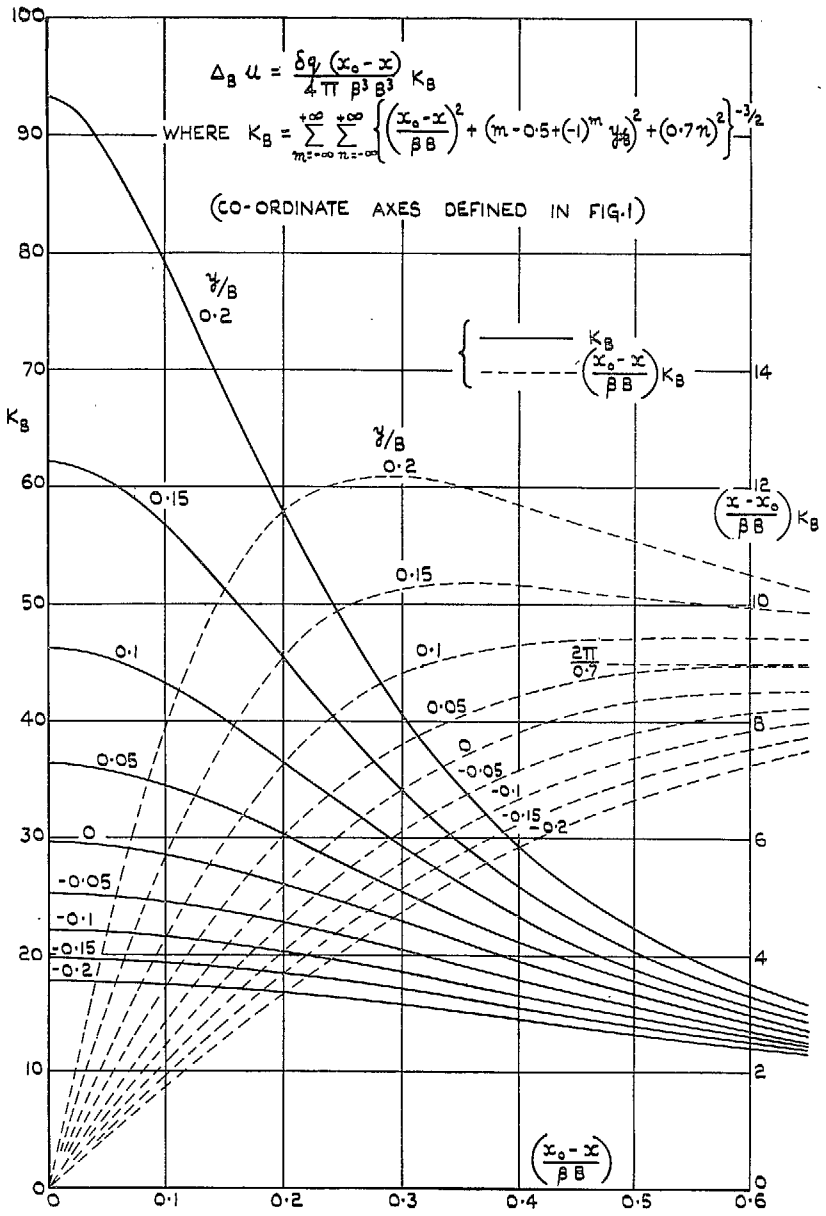

FIG. 3. Increment in velocity, $\Delta_B u$, at $(x_0, 0{\cdot}5B, 0)$ on the side wall due to a source, δq, at $(x, y, 0)$ and its images in a rectangular tunnel $(B \times 0{\cdot}7B)$.

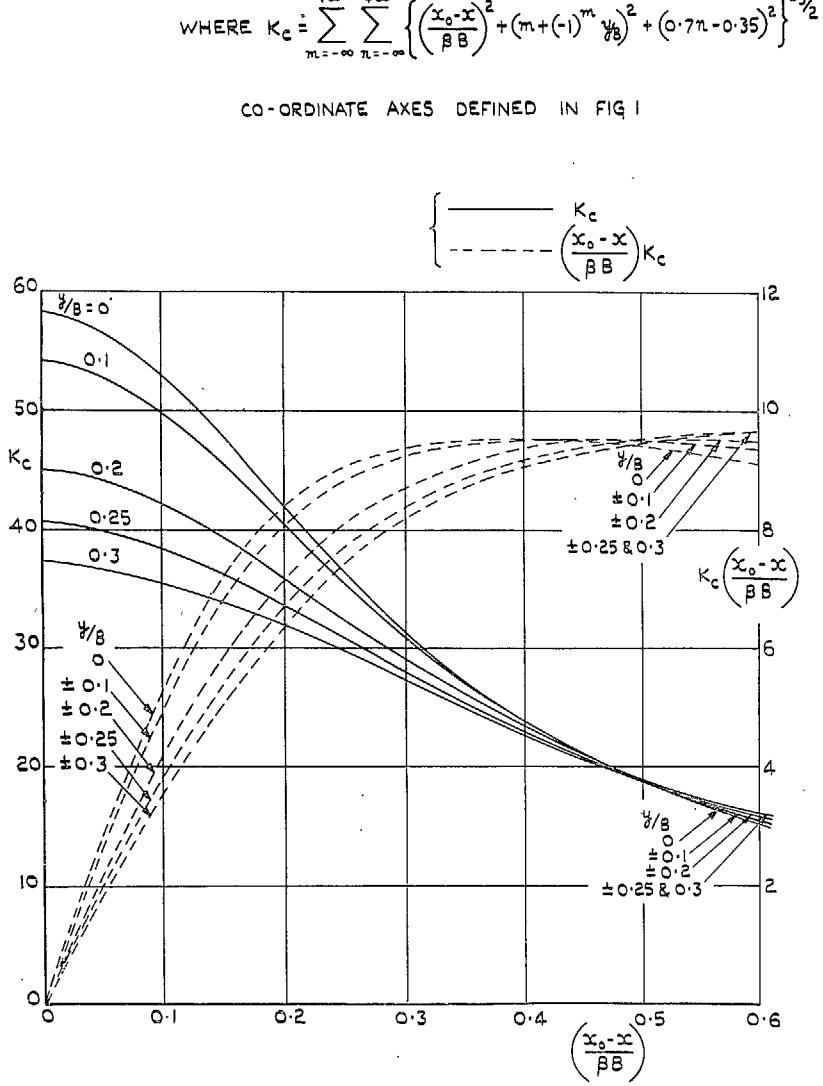

FIG. 4. Increment in velocity, $\Delta_C u$, at $(x_0, 0, 0{\cdot}35B)$ on the top wall due to a source, δq, at $(x, y, 0)$ and its images in a rectangular tunnel $(B \times 0{\cdot}7B)$.

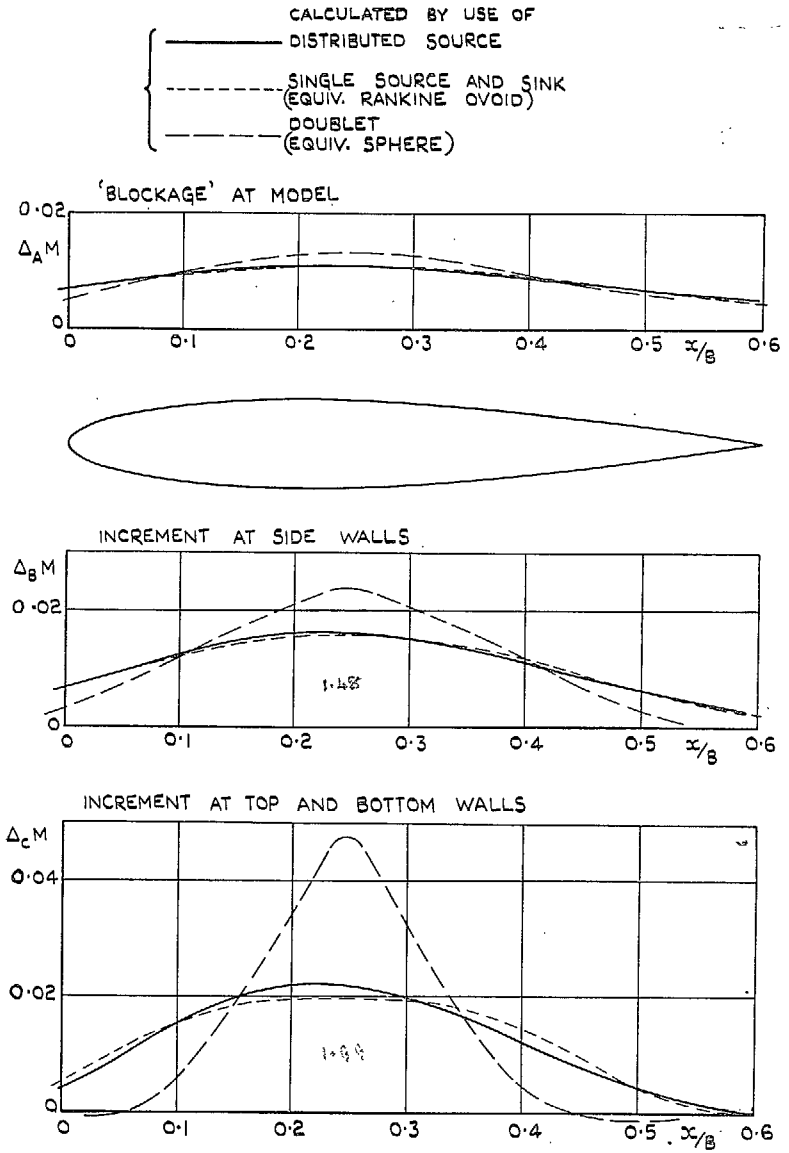

FIG. 5. Comparison of calculated increments in Mach number due to a body represented by a continuous source distribution, by an equivalent Rankine ovoid and by an equivalent sphere (body of length $0{\cdot}6B$ at $M = 0{\cdot}85$).

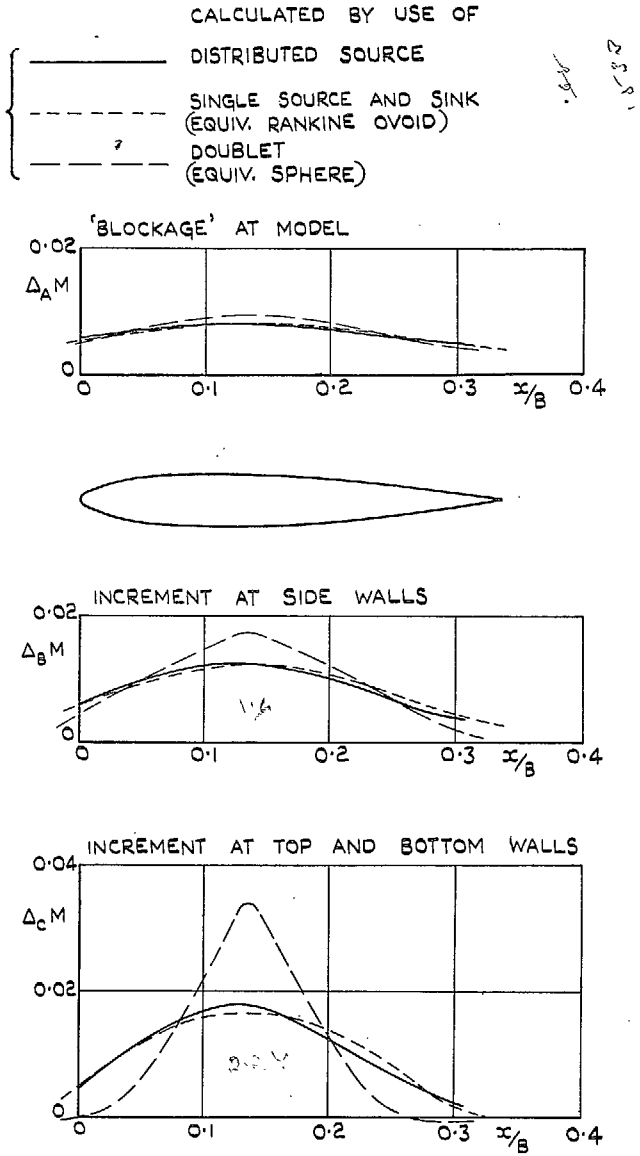

FIG. 6. Comparison of calculated increments in Mach number due to a body represented by a continuous source distribution, by an equivalent Rankine ovoid and by an equivalent sphere (body of length $0{\cdot}33B$ at $M = 0{\cdot}94$).

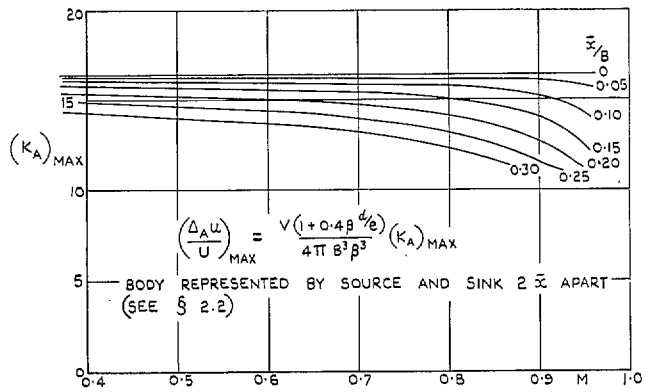

FIG. 7. Variation of $(K_A)_{max}$ with Mach number at constant $\bar{x}/B$.

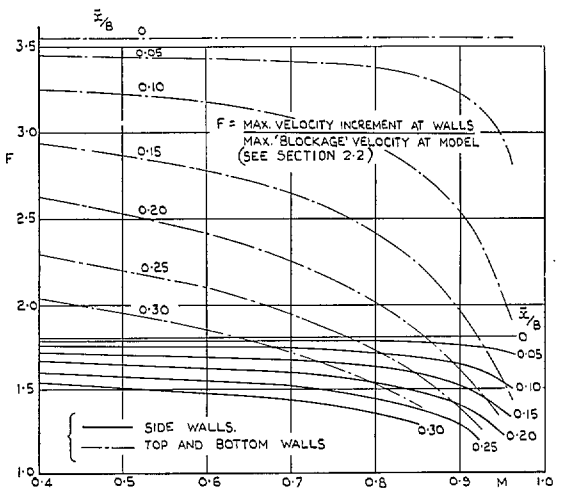

FIG. 8. Variation of $F\left(= \frac{\text{max. wall velocity increment}}{\text{max. centre-line velocity increment}}\right)$ with Mach number at constant $\bar{x}/B$.

CALCULATION FOR NONTAPERED WING OF SPAN 0·2B (ASSUMING SOURCE & SINK 0·08B APART)

CAN BE APPLIED TO ANY WING OF SAME MEAN SWEEP FOR WHICH $2\sqrt{3}\,k_1 = 0{\cdot}2B$ WHERE k_1 IS THE RADIUS OF GYRATION ABOUT THE ROLL AXIS

$$\frac{\Delta u_A}{U} = \frac{V(1+1{\cdot}2\beta^{b/c}+14\Delta C_D)\,\bar{K}_A}{4\pi B^3\beta^3}$$

$\phi_M = \tan^{-1}\left\{\frac{1}{\beta}\tan\phi\right\}$ WHERE ϕ IS THE MEAN ANGLE OF SWEEP

x_0 IS DISTANCE DOWNSTREAM OF MIDPOINT HALF CHORD LINE

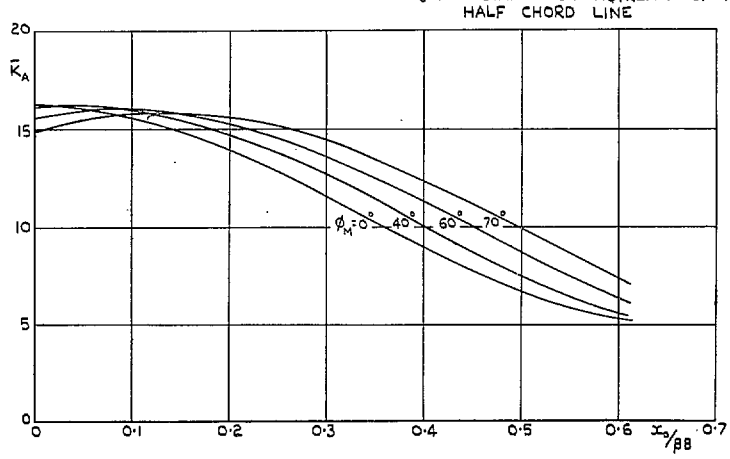

FIG. 9a. Distribution of blockage increments in velocity along the centre-line of the tunnel due to a wing for which $2\sqrt{3}k_1 = 0{\cdot}2B$.

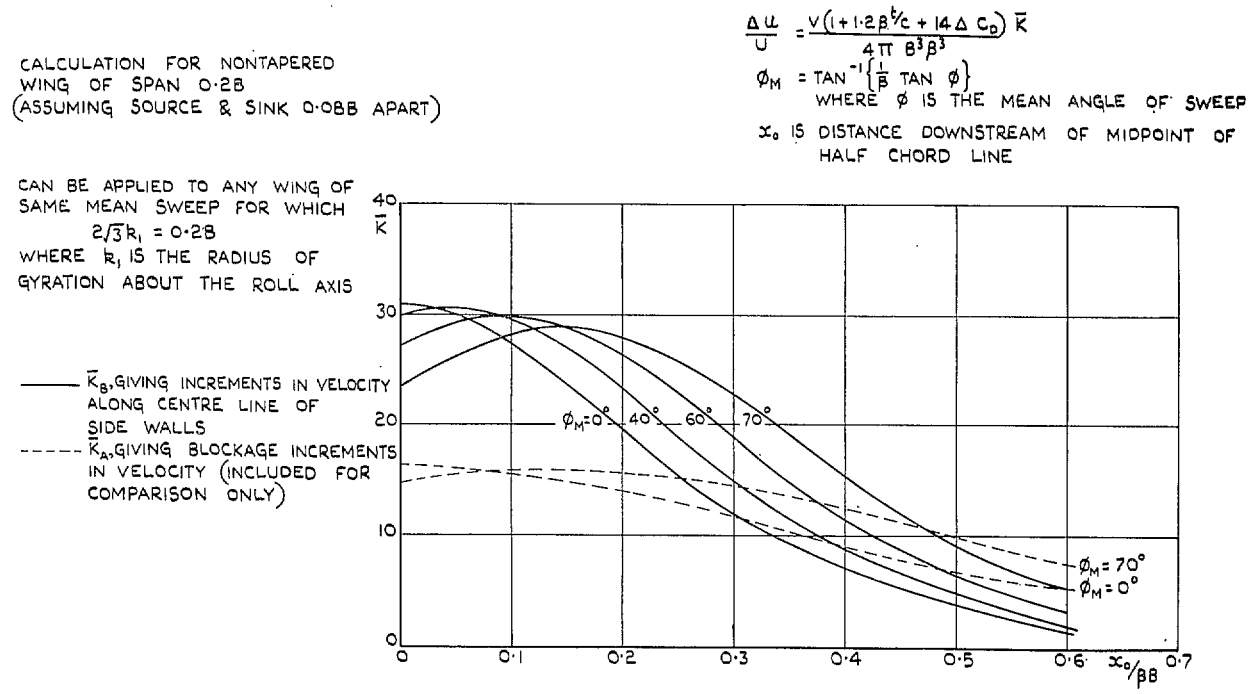

FIG. 9b. Distribution of increments in velocity on the side walls due to a wing for which $2\sqrt{3}k_1 = 0{\cdot}2B$.

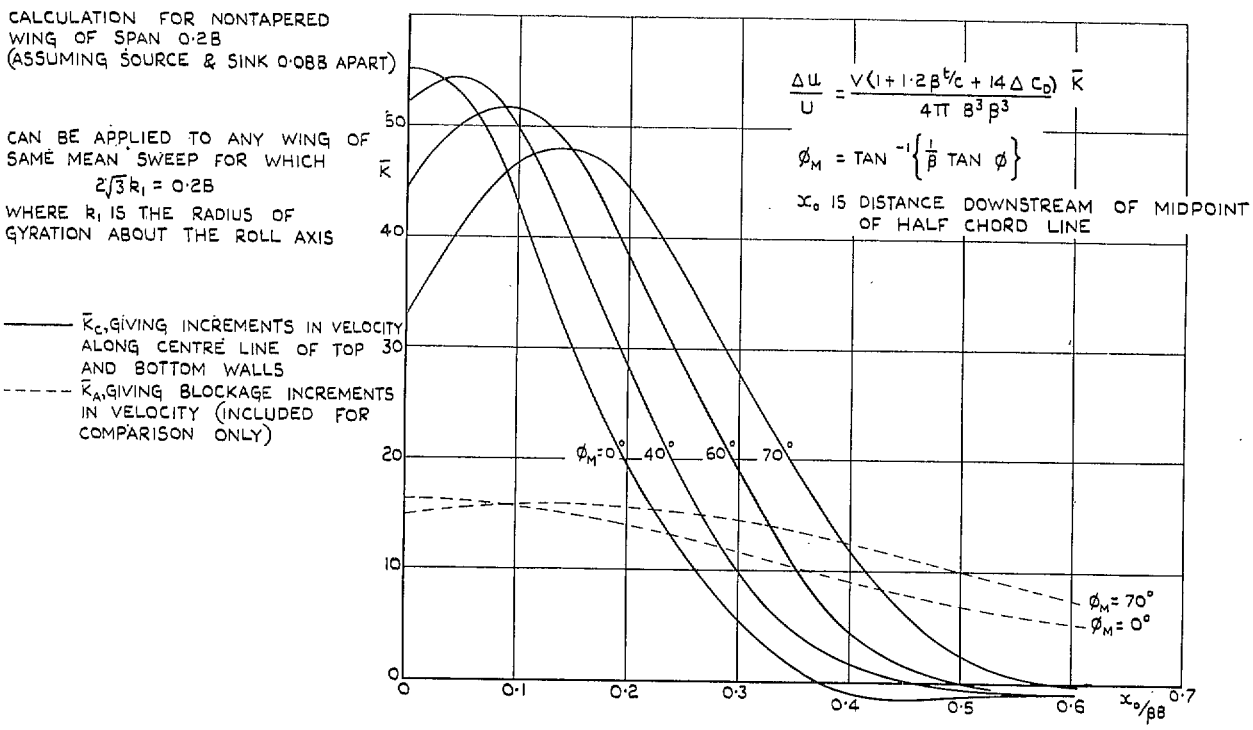

FIG. 9c. Distribution of increments in velocity on top and bottom walls due to a wing for which $2\sqrt{3}k_1 = 0{\cdot}2B$.

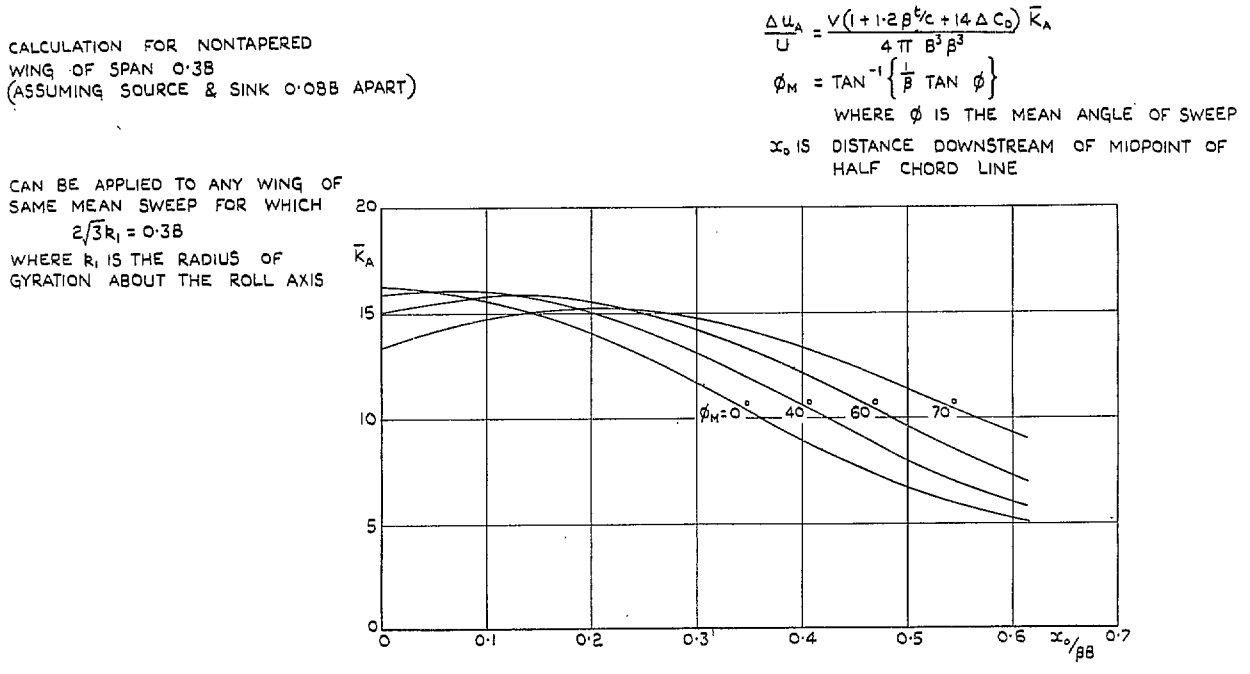

FIG. 10a. Distribution of blockage increments in velocity along the centre-line of the tunnel due to a wing for which $2\sqrt{3}k_1 = 0{\cdot}3B$.

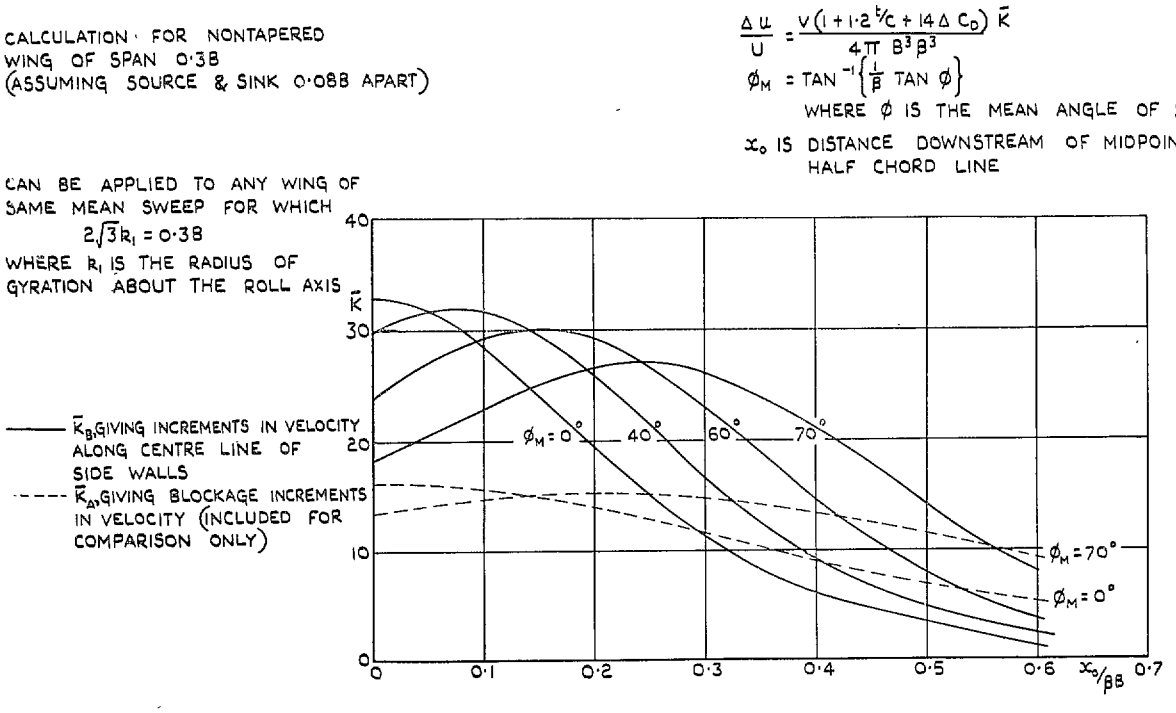

FIG. 10b. Distribution of increments in velocity on the side walls due to a wing for which $2\sqrt{3}k_1 = 0{\cdot}3B$.

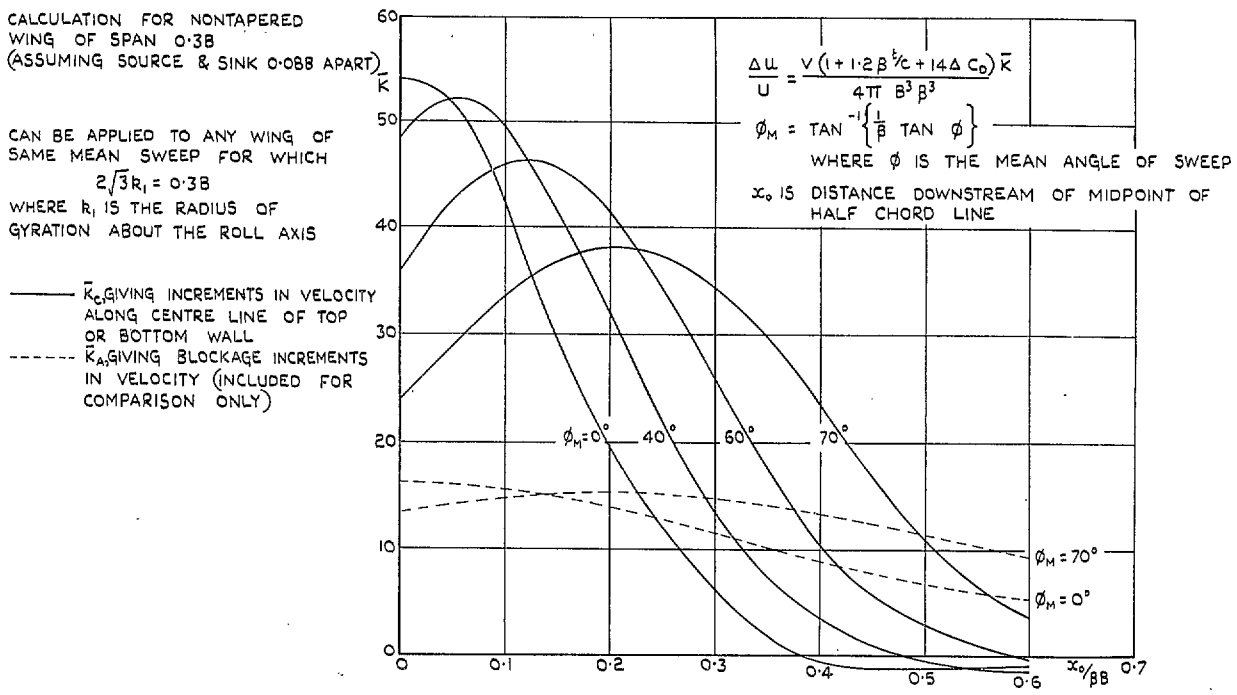

FIG. 10c. Distribution of increments in velocity on the top and bottom walls due to a wing for which $2\sqrt{3}k_1 = 0{\cdot}3B$.

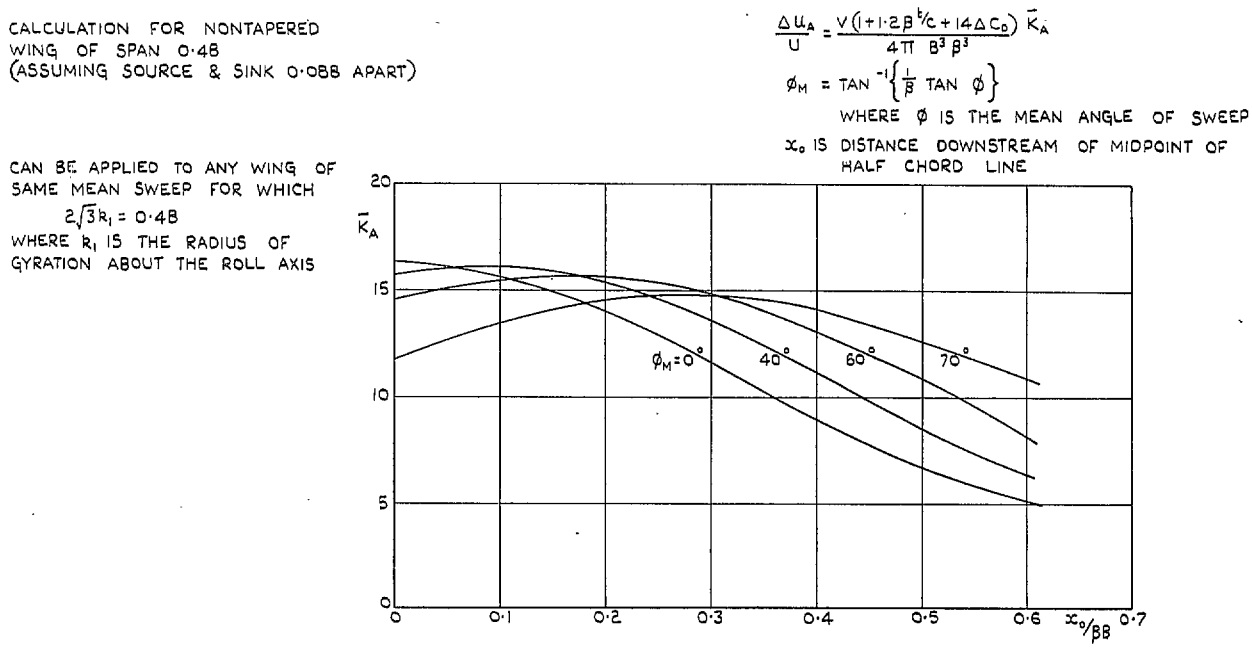

FIG. 11a. Distribution of blockage increments in velocity along the centre-line of the tunnel due to a wing for which $2\sqrt{3}k_1 = 0{\cdot}4B$.

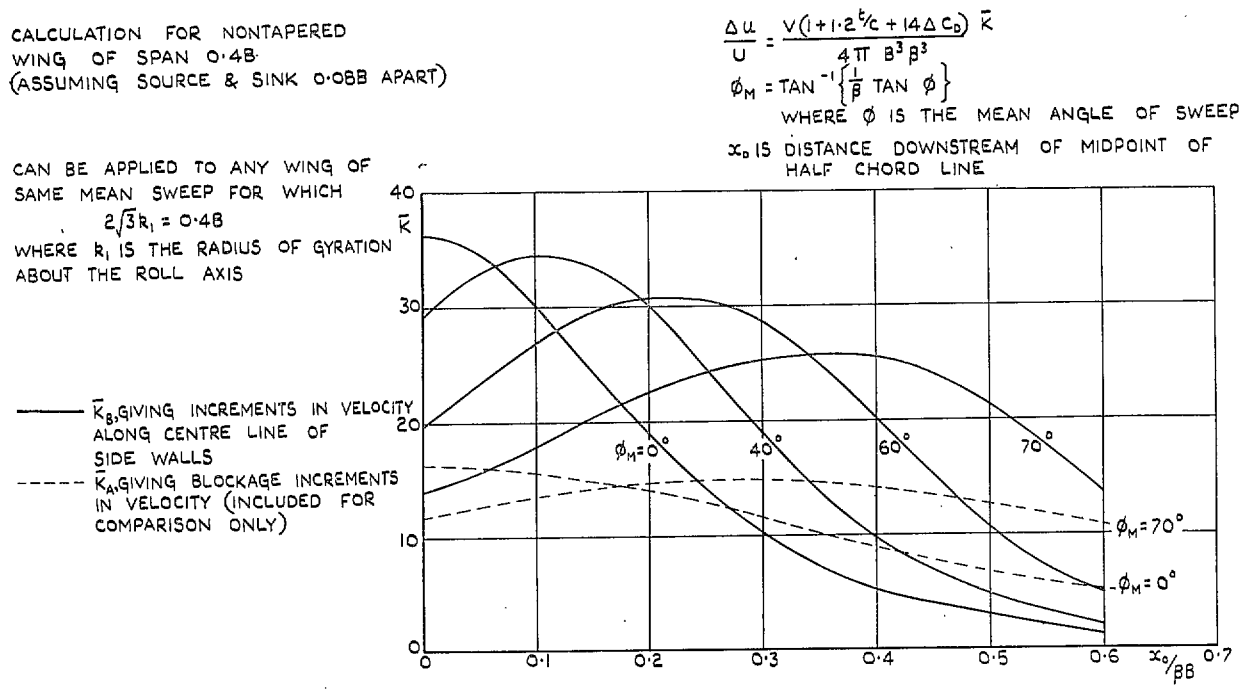

FIG. 11b. Distribution of increments in velocity on the side walls due to a wing for which $2\sqrt{3}k_1 = 0{\cdot}4B$.

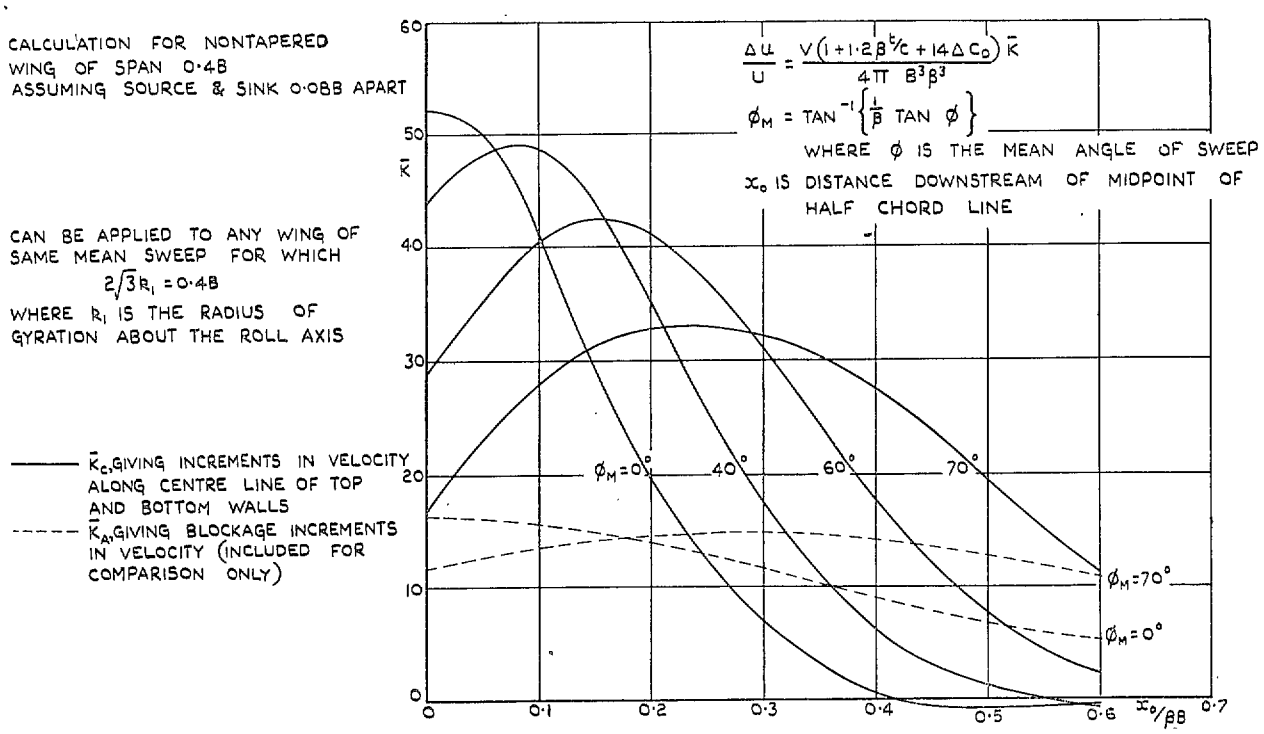

FIG. 11c. Distribution of increments in velocity on the top and bottom walls due to a wing for which $2\sqrt{3}k_1 = 0{\cdot}4B$.

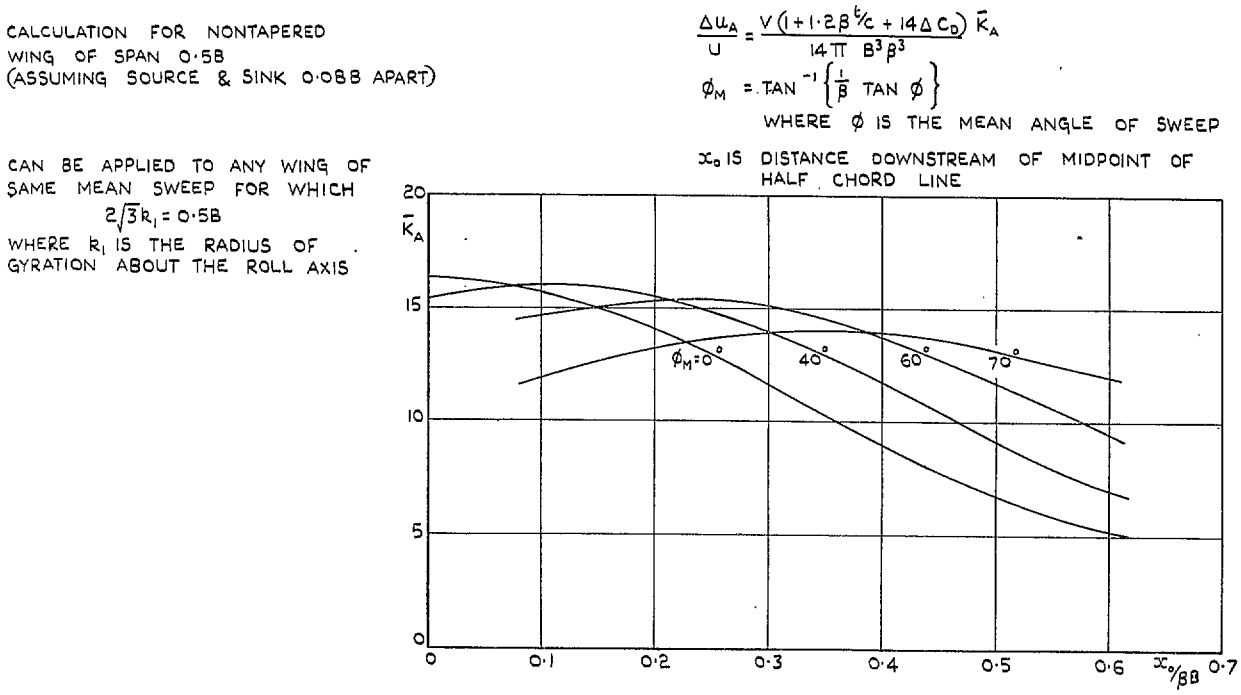

FIG. 12a. Distribution of blockage increments in velocity along the centre-line of the tunnel due to a wing for which $2\sqrt{3}k_1 = 0{\cdot}5B$.

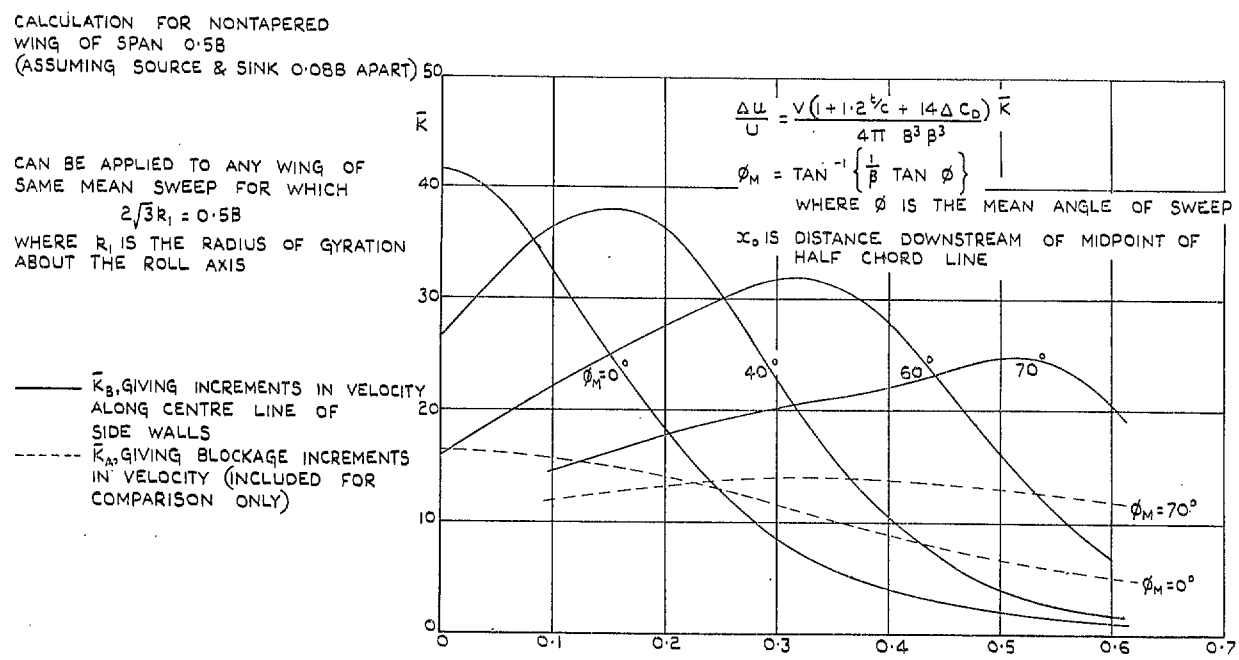

FIG. 12b. Distribution of increments in velocity on the side walls due to a wing for which $2\sqrt{3}k_1 = 0{\cdot}5B$.

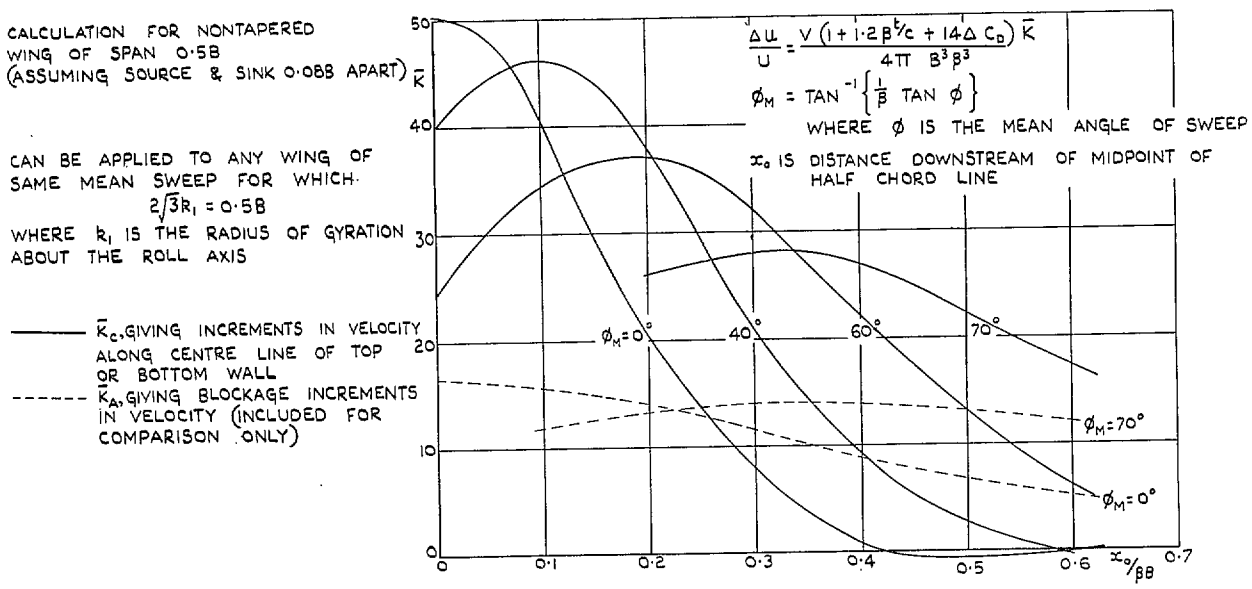

FIG. 12c. Distribution of increments in velocity on the top and bottom walls due to a wing for which $2\sqrt{3}k_1 = 0{\cdot}5B$.

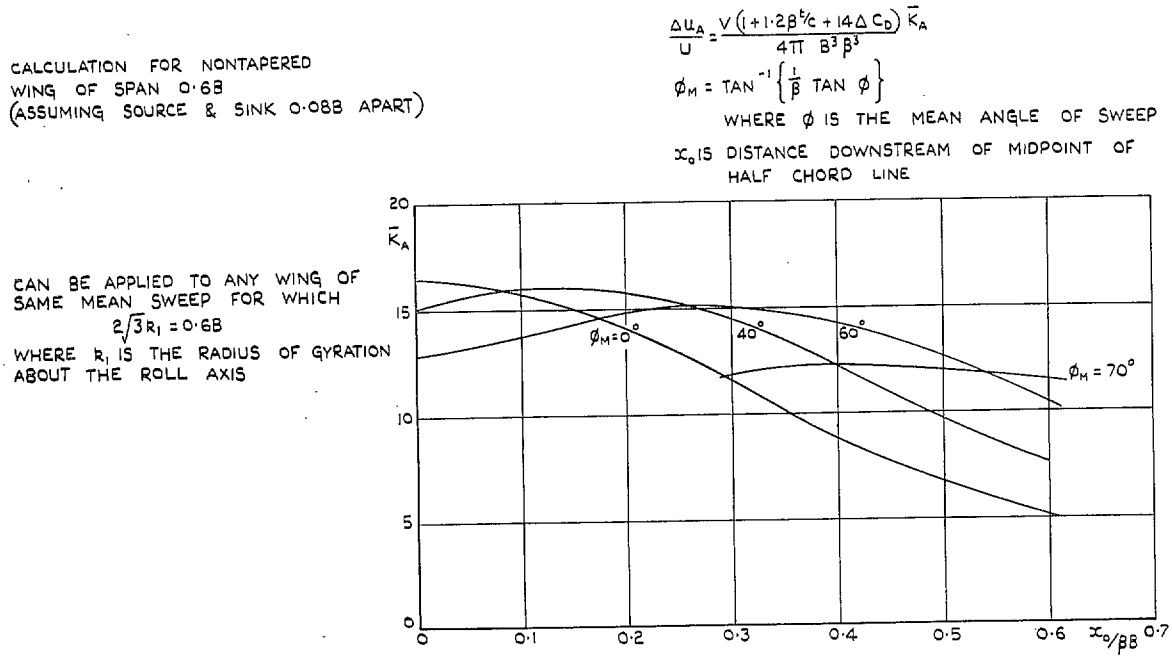

FIG. 13a. Distribution of blockage increments in velocity along the centre-line of the tunnel due to a wing for which $2\sqrt{3}k_1 = 0{\cdot}6B$.

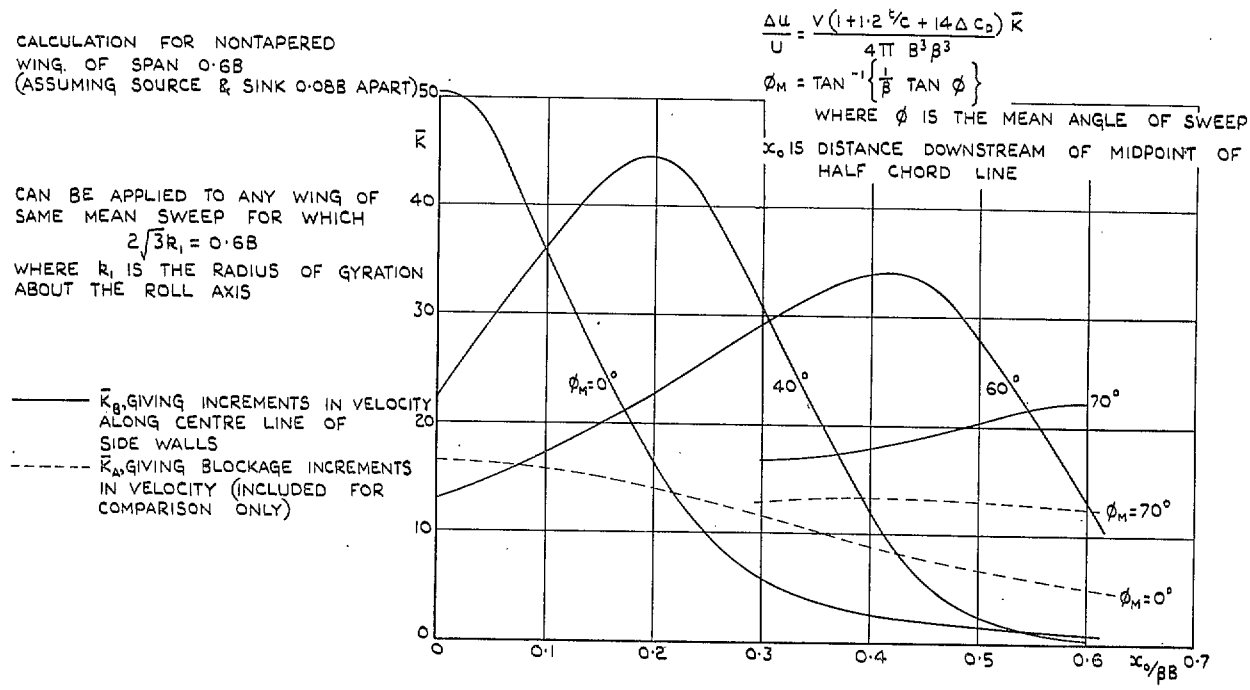

FIG. 13b. Distribution of increments in velocity on the side walls due to a wing for which $2\sqrt{3}k_1 = 0·6B$.

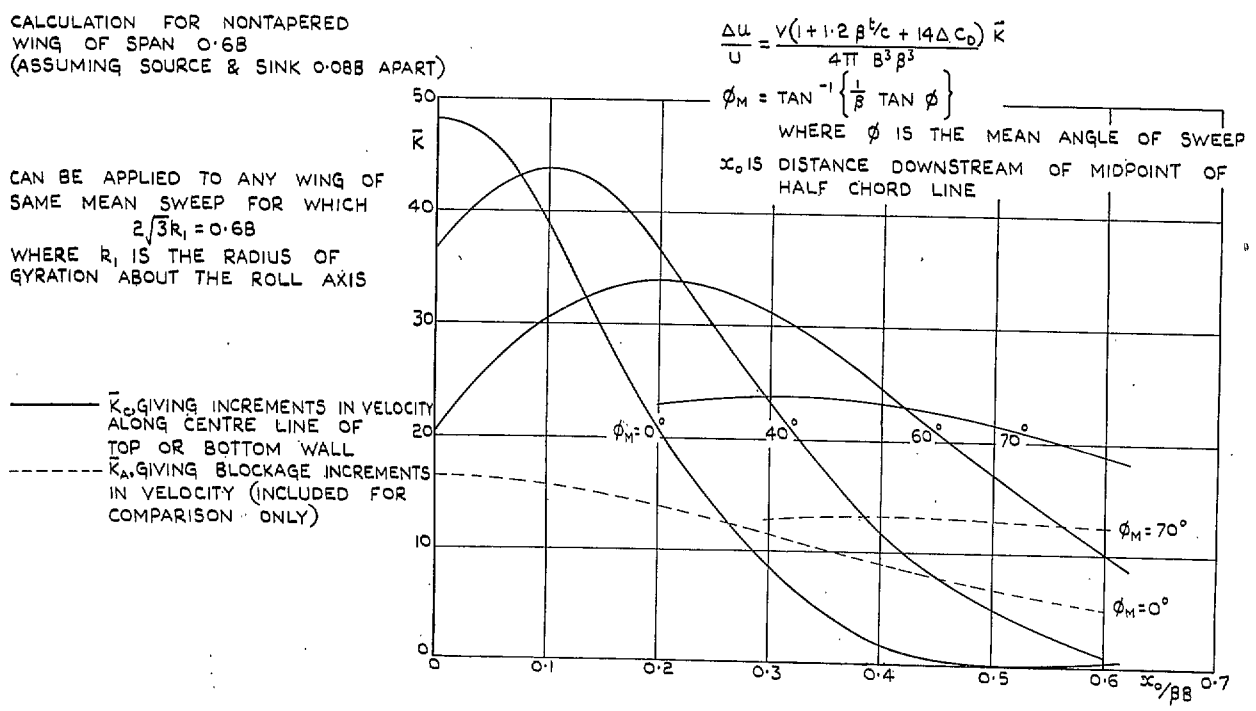

FIG. 13c. Distribution of increments in velocity on top and bottom walls due to a wing for which $2\sqrt{3}k_1 = 0·6B$.

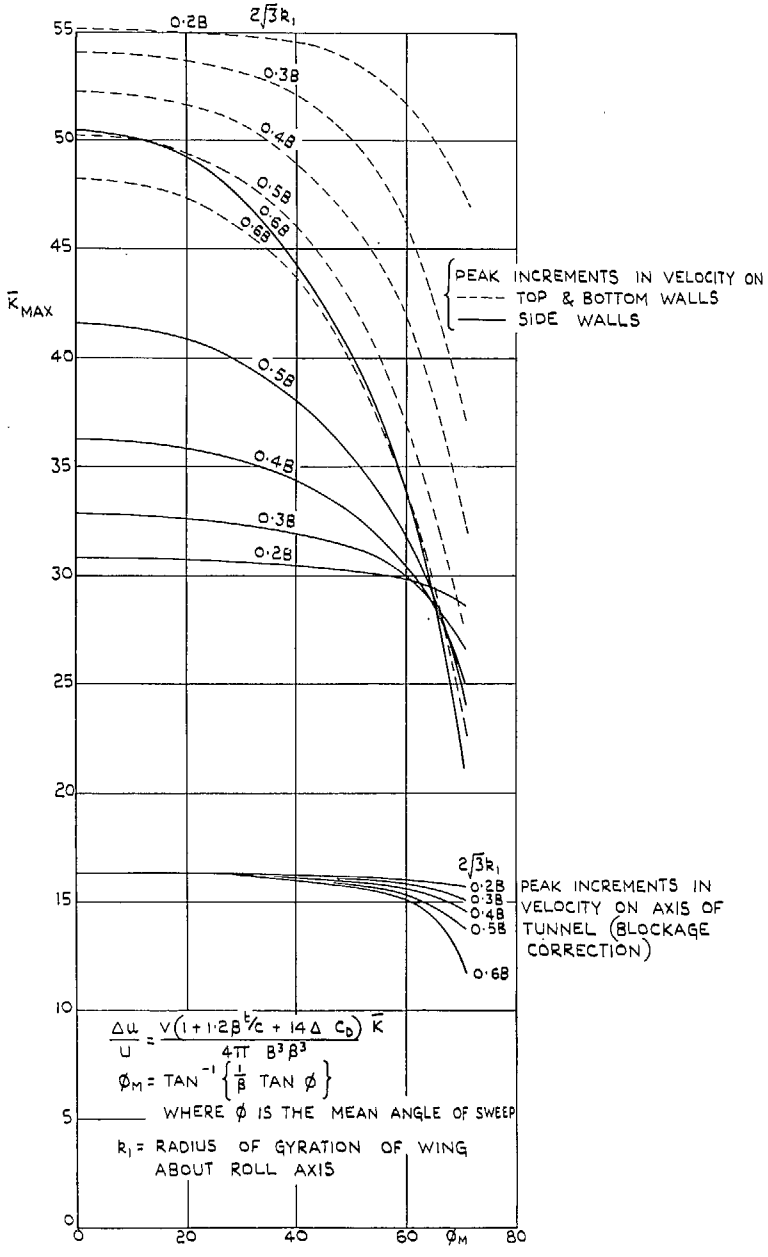

FIG. 14. Peak increments in velocity due to wings of various span and sweepback.

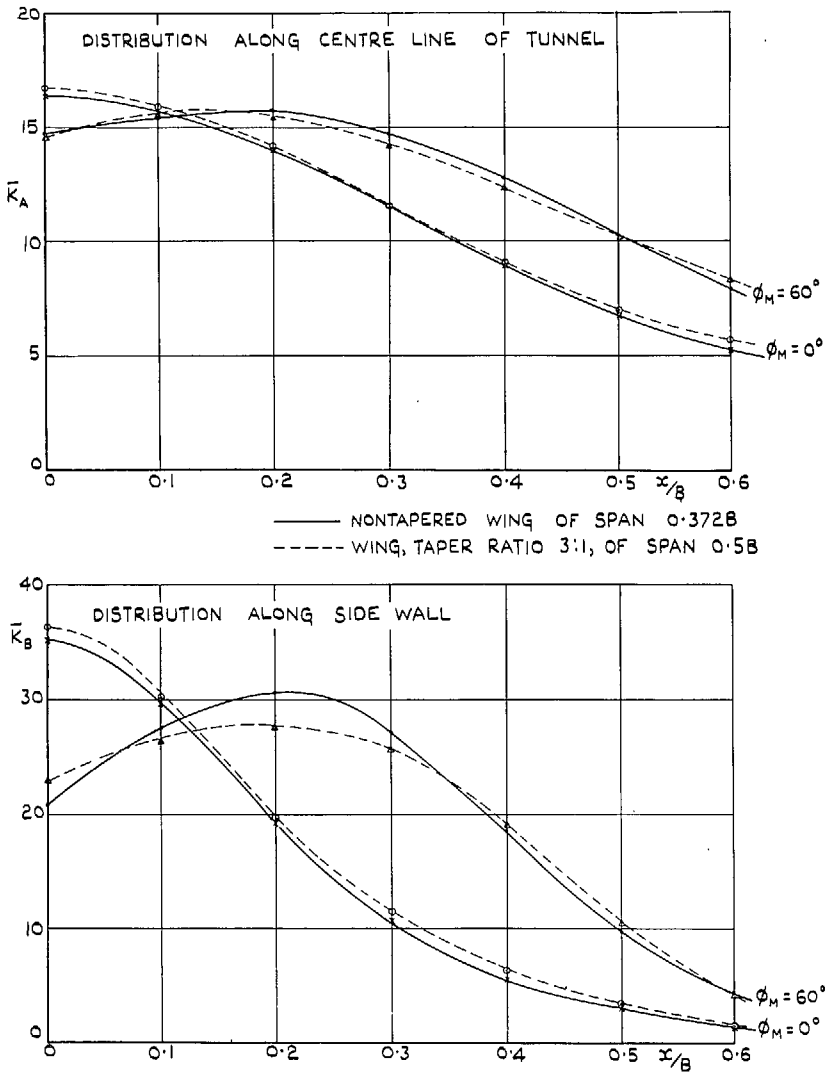

FIG. 15. Comparison of increments in velocity due to tapered wings (taper ratio 3 : 1) of span $0{\cdot}5B$ and non-tapered wings of equal volume, mean angle of sweep and thickness/chord ratio, having the same radius of gyration about the roll axis.

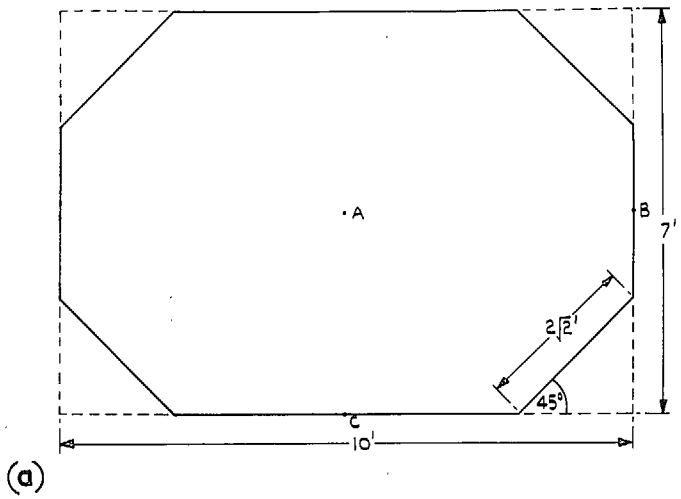

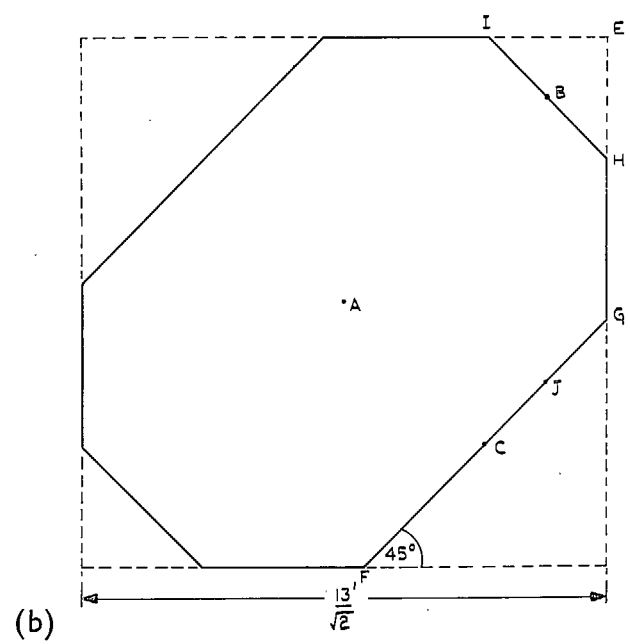

FIG. 16. Cross-section of the R.A.E. High Speed Tunnel.

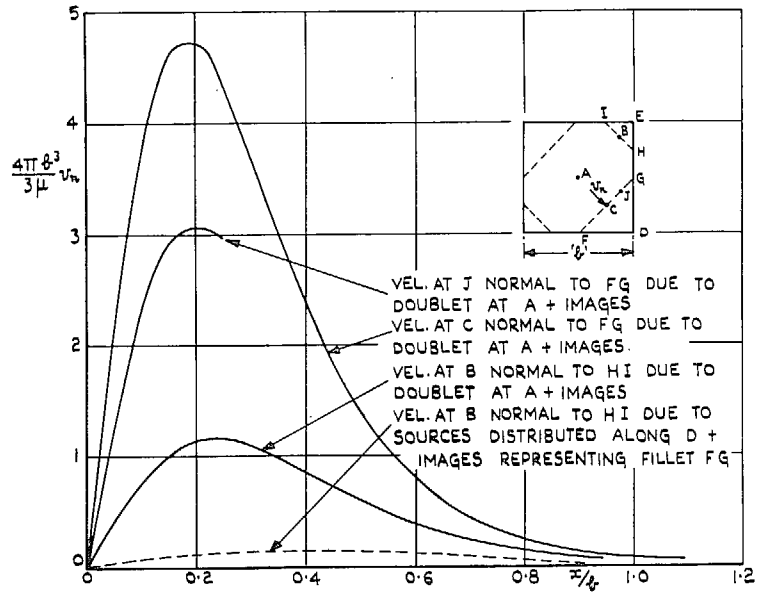

FIG. 17. Longitudinal distribution of transverse velocities induced by a doublet on the axis of a square tunnel.

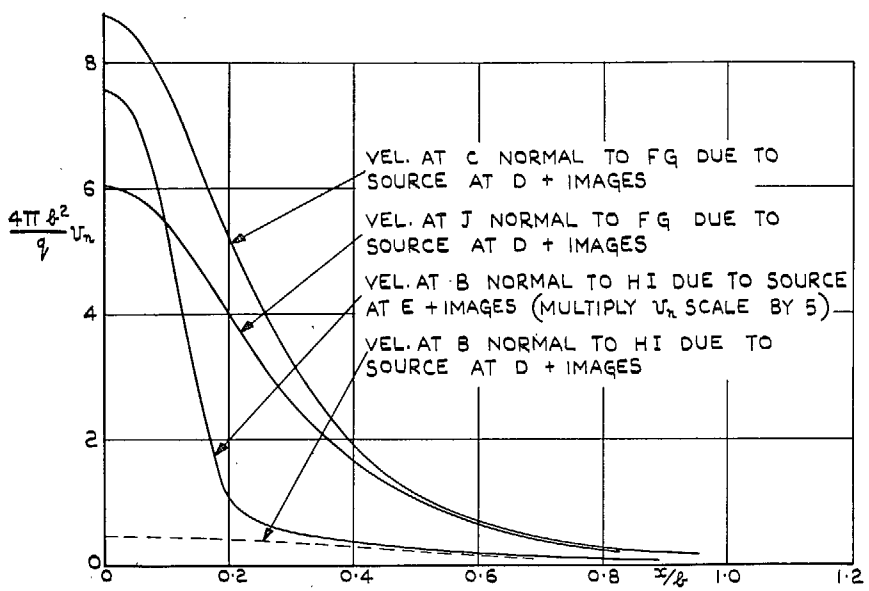

FIG. 18. Longitudinal distribution of transverse velocities induced by a source on the corner of a square tunnel.

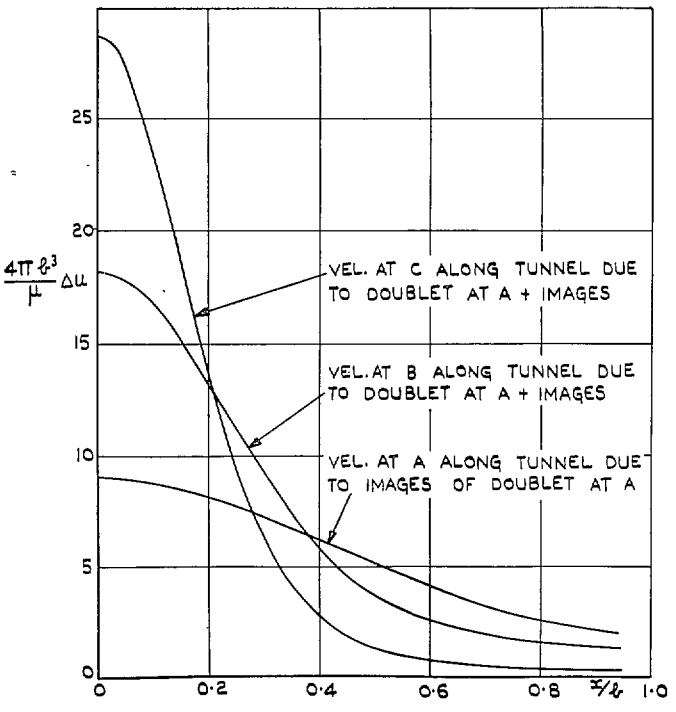

FIG. 19. Longitudinal distribution of velocities along tunnel induced by a doublet on the axis of a square tunnel.

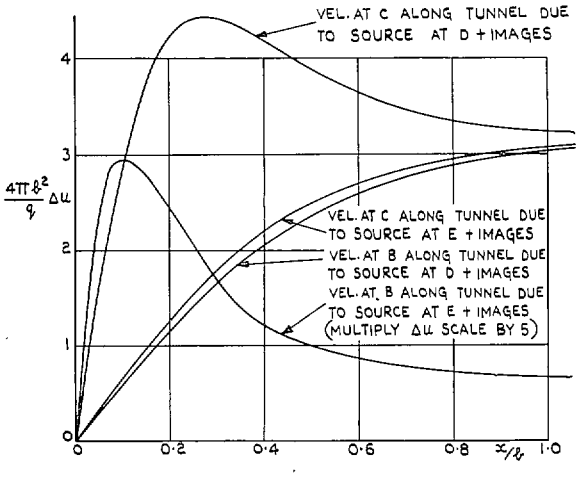

FIG. 20. Longitudinal distribution of velocities along tunnel induced by a source on the corner of a square tunnel.

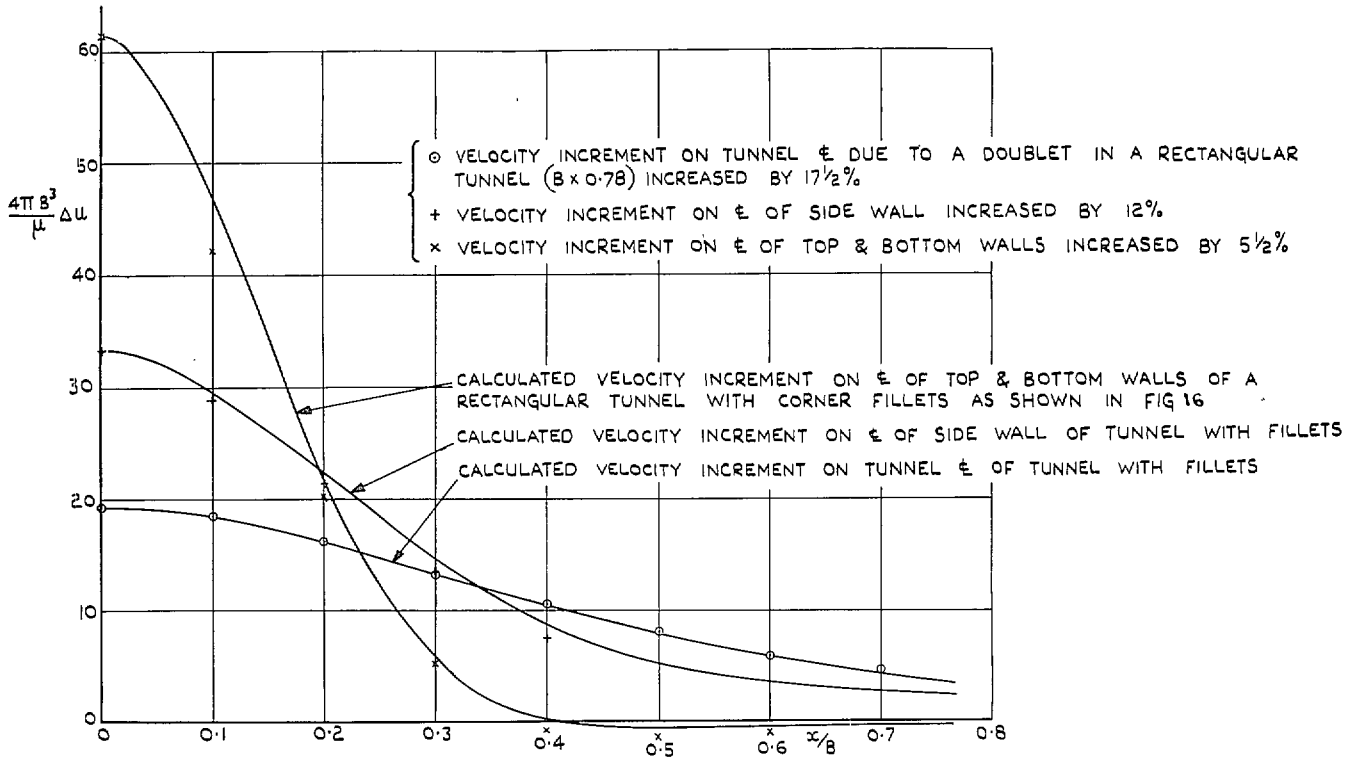

FIG. 21. Comparison of velocity increments due to a doublet in a rectangular tunnel with corner fillets with those for a tunnel without fillets increased by an overall factor.

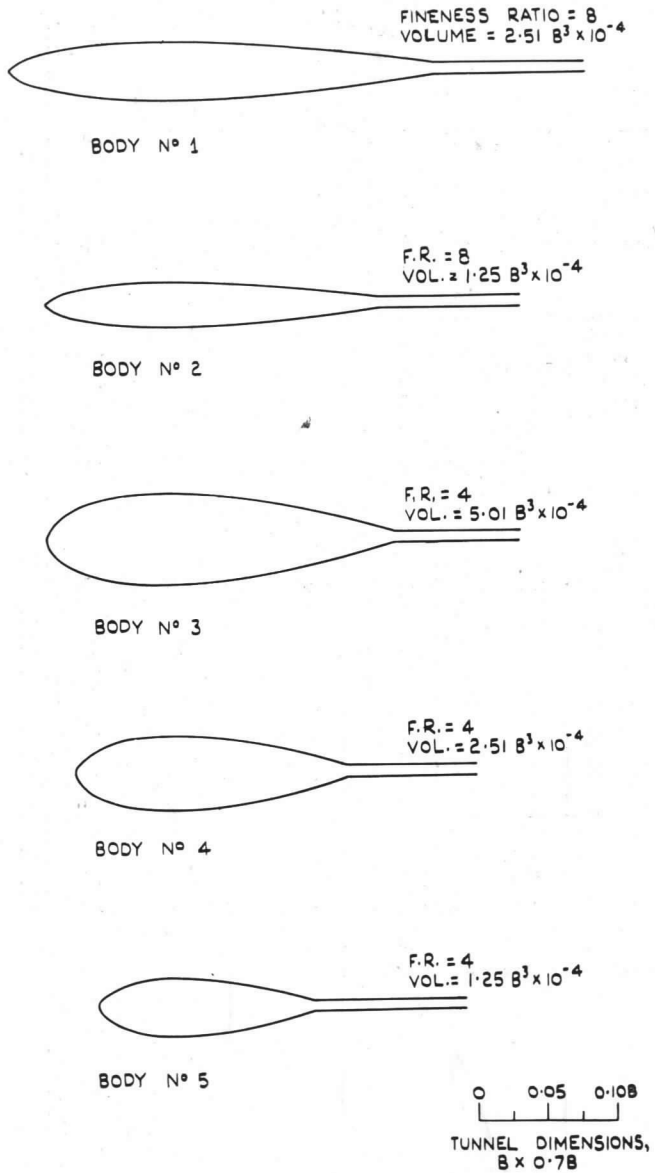

FIG. 22. Family of bodies of revolution of the same shape but different sizes (used in tests described in section 5).

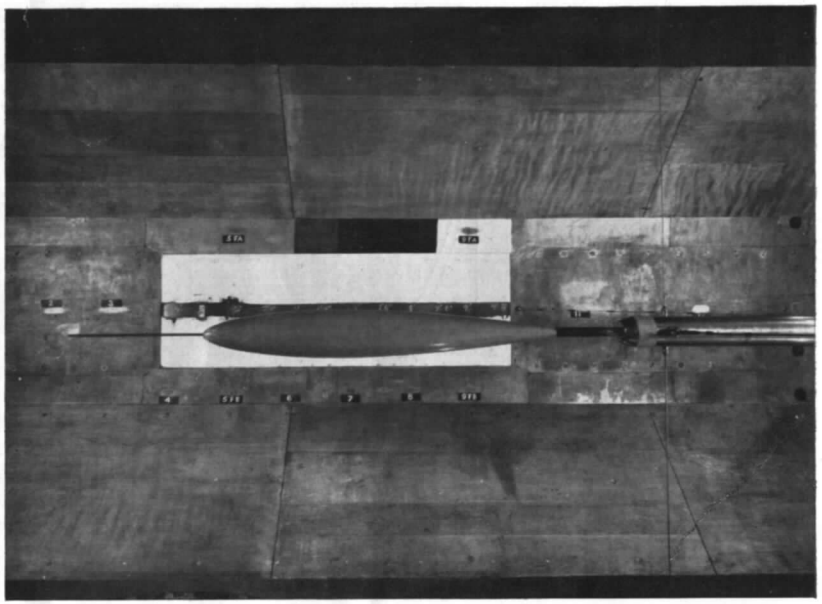

Side View

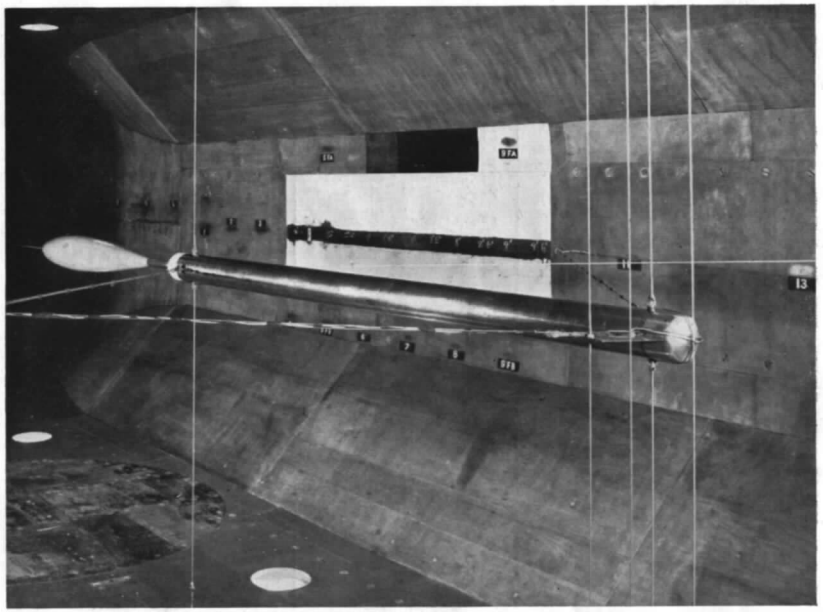

Rear View

FIG. 23. Rig used in experiments on bodies of revolution of same shape but of different sizes.

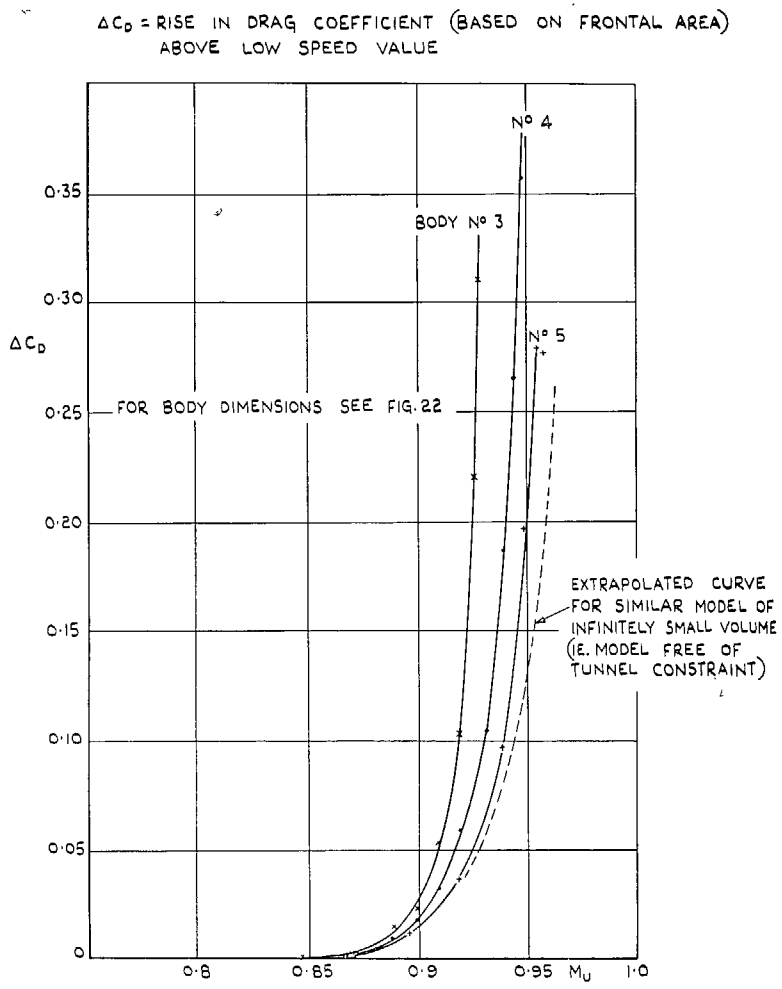

FIG. 24. Measurements of drag on bodies of same shape but of different sizes.

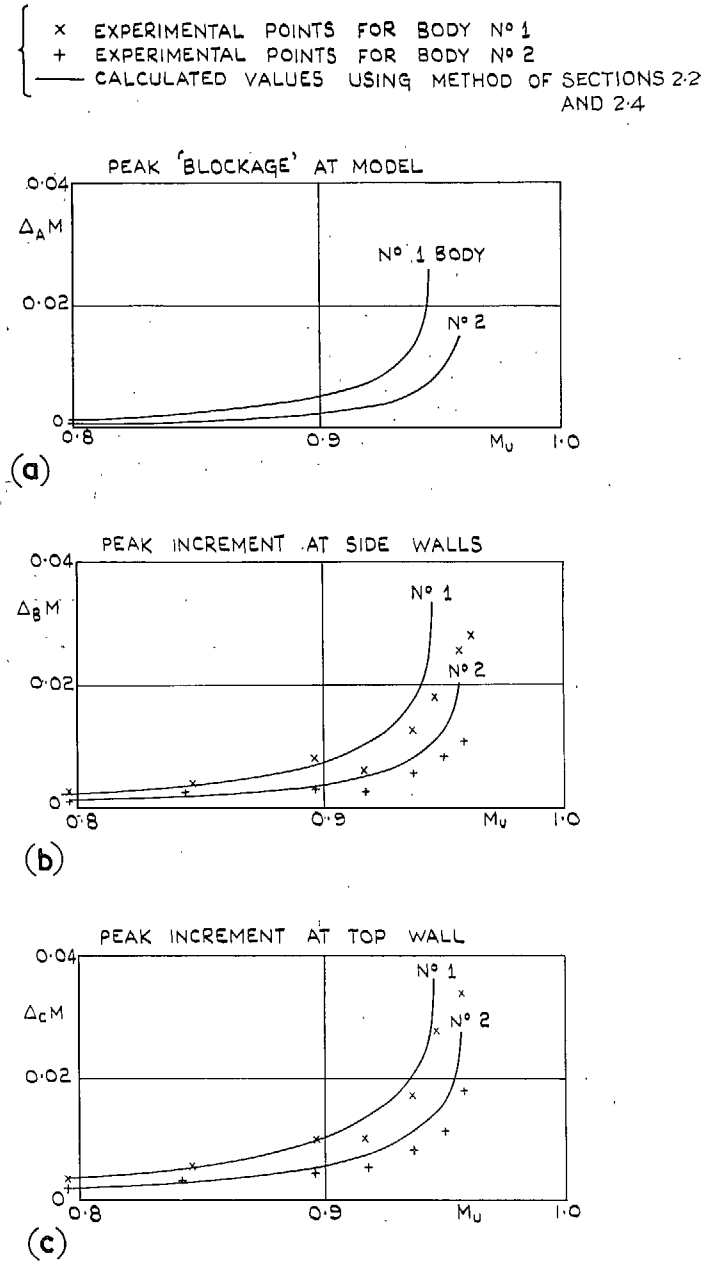

FIG. 25a to 25c. Comparison of measured and calculated peak increments in Mach number for bodies 1 and 2.

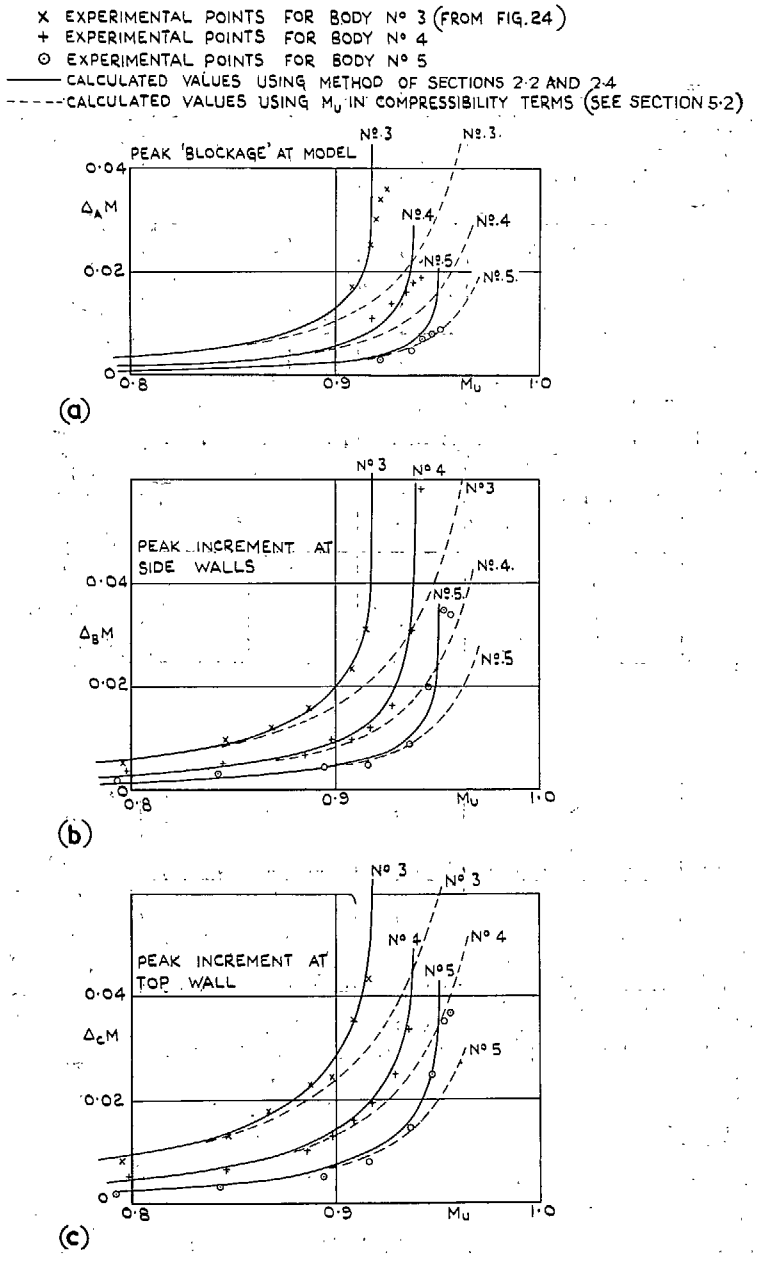

FIG. 26a to 26c. Comparison of measured and calculated peak increments in Mach number for bodies 3, 4 and 5.

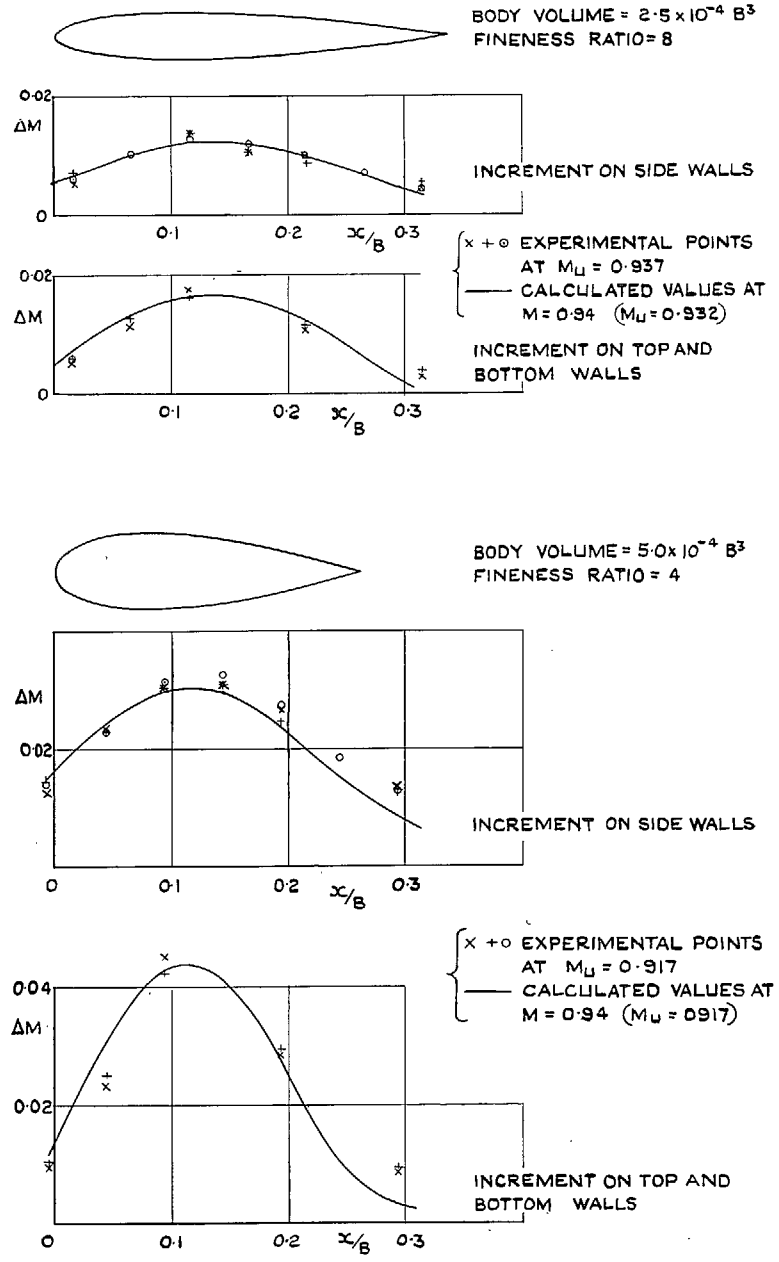

FIG. 27. Comparison of measured and calculated longitudinal distribution of velocity increment due to two bodies of revolution.

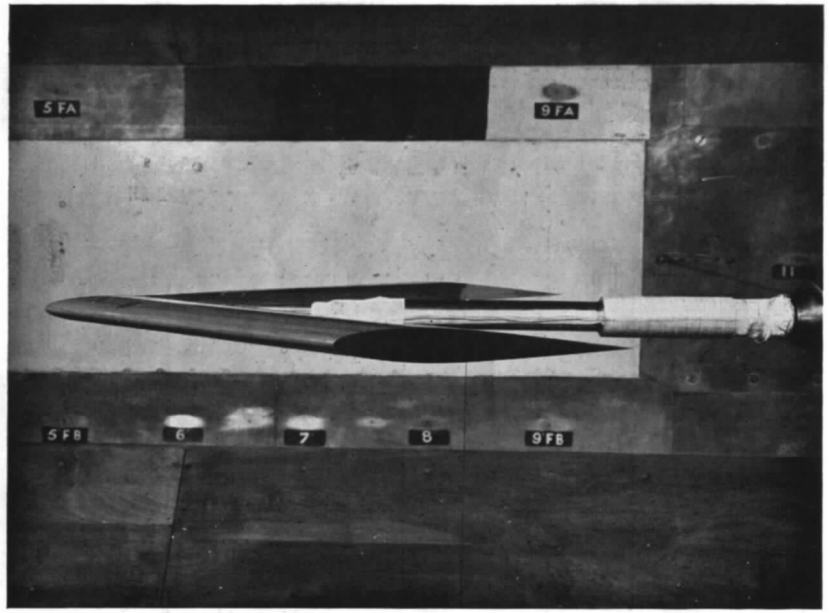

Side View

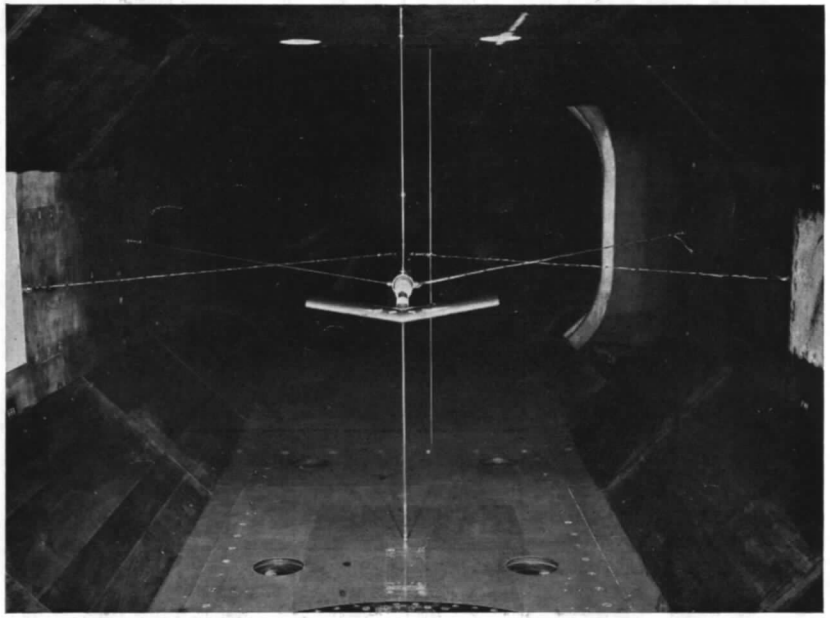

Front View

FIG. 28. Rig used in experiments on non-tapered wings of various span and sweep-back.

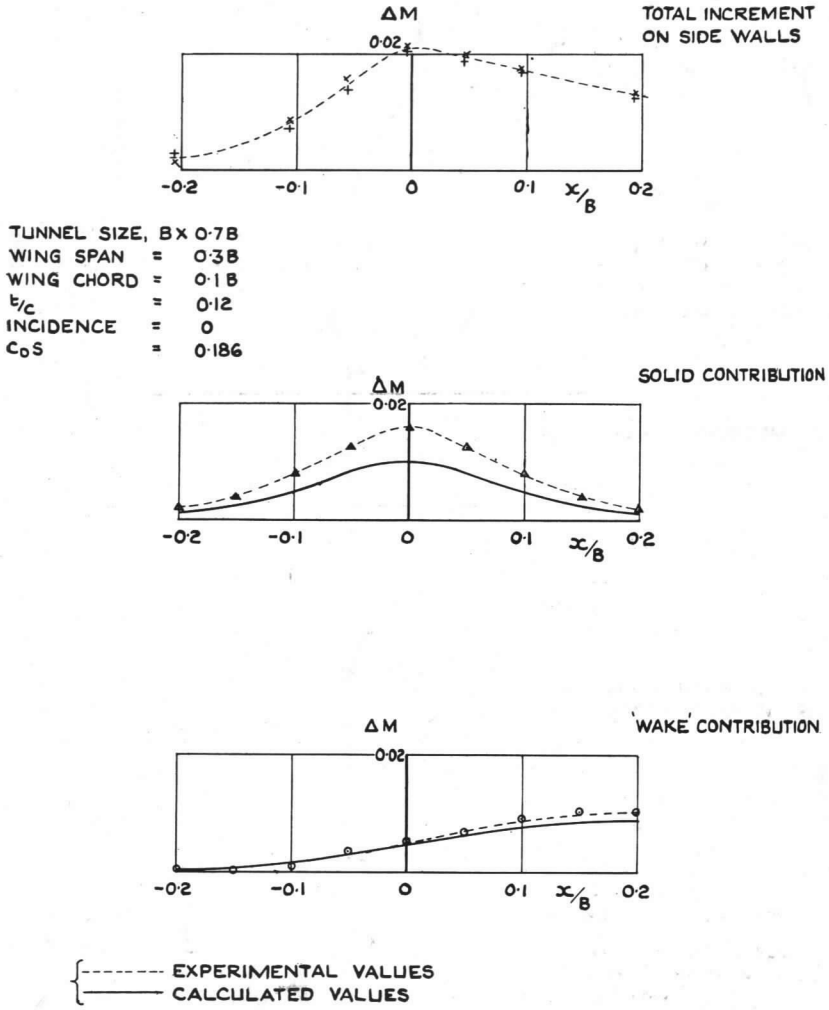

FIG. 29. Comparison of measured and calculated longitudinal distribution of velocity increment on the side walls due to an unswept wing at $M_u = 0{\cdot}895$.

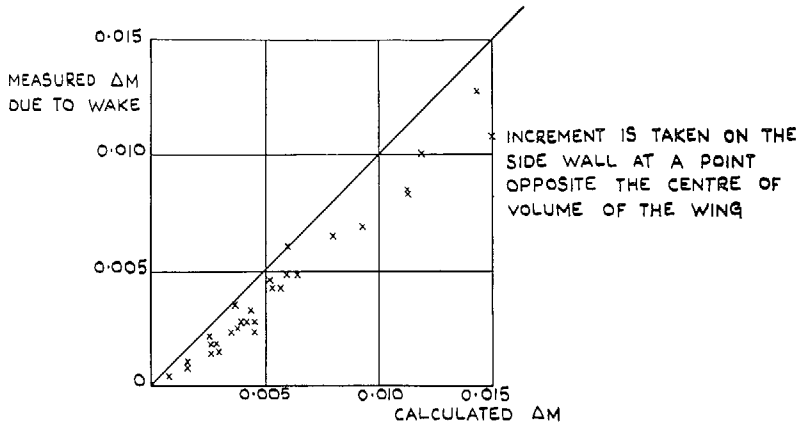

FIG. 30. Comparison of measured and calculated velocity increments on the side wall due to wakes of a series of wings of various span and sweep at various incidences and Mach numbers.

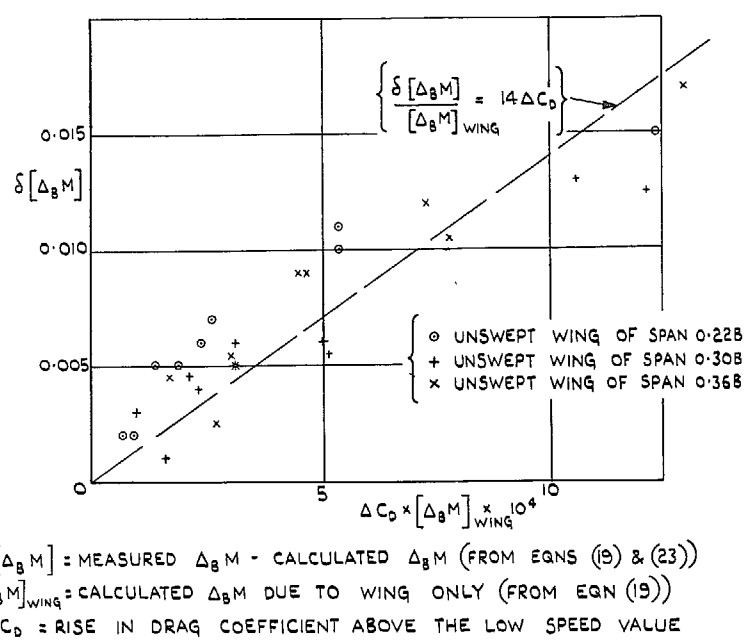

FIG. 31. Relationship between under-estimate of peak wall increments in Mach number due to wing and rise in drag coefficient.

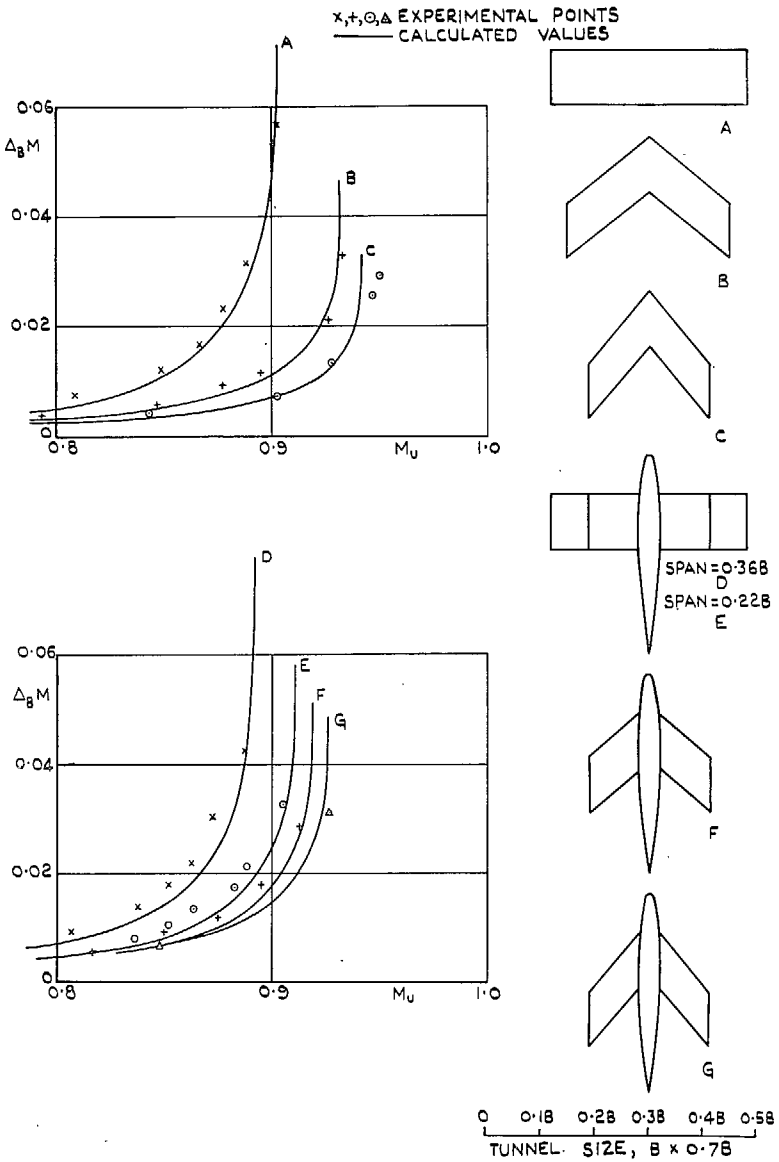

FIG. 32a. Comparison of measured and calculated peak increments in Mach number on side wall due to various models.

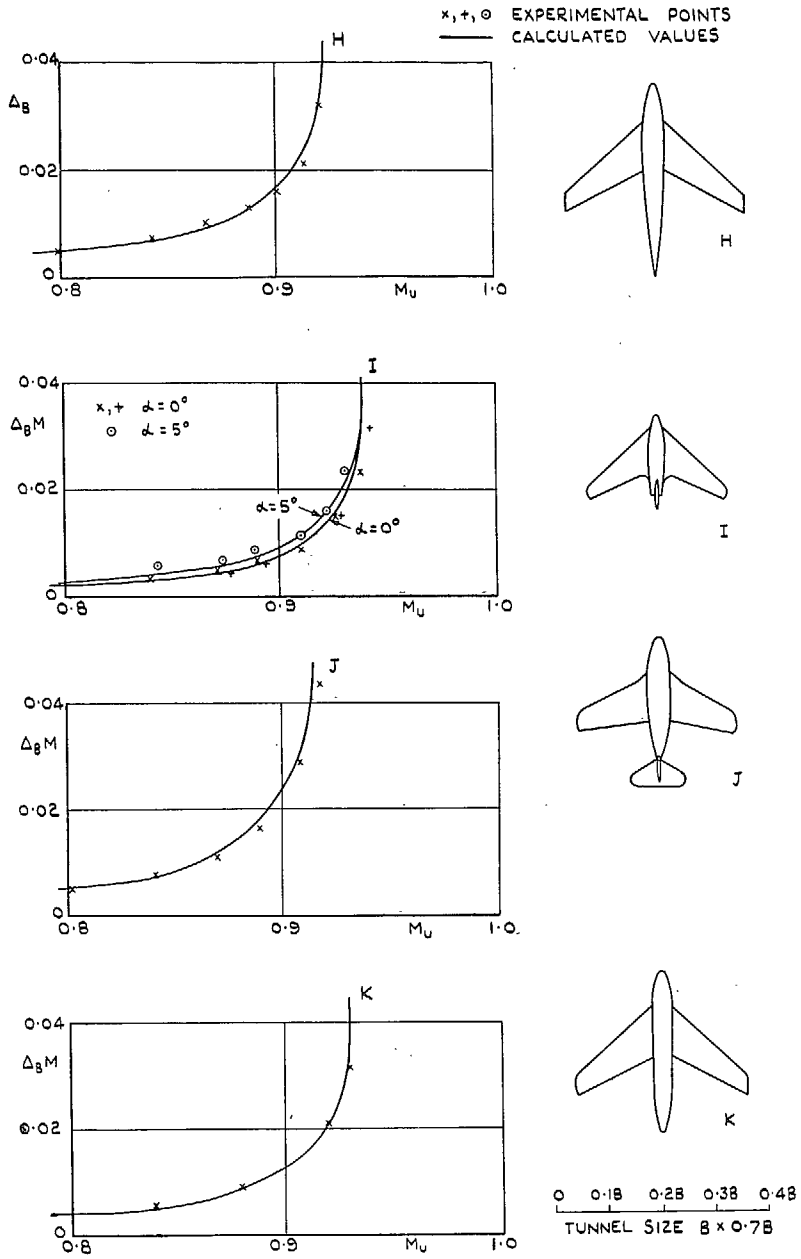

FIG. 32b. Comparison of measured and calculated peak increments in Mach number on side wall due to various models.

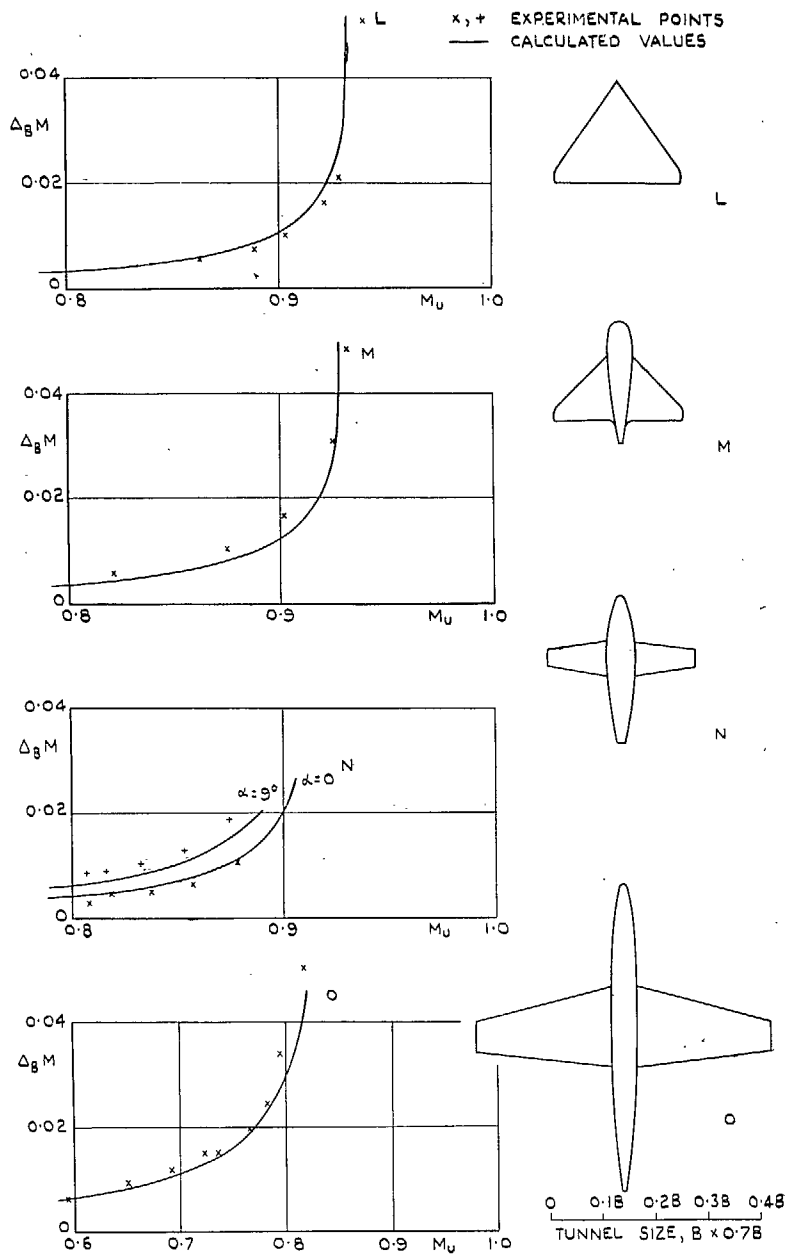

FIG. 32c. Comparison of measured and calculated peak increments in Mach number on side wall due to various models.

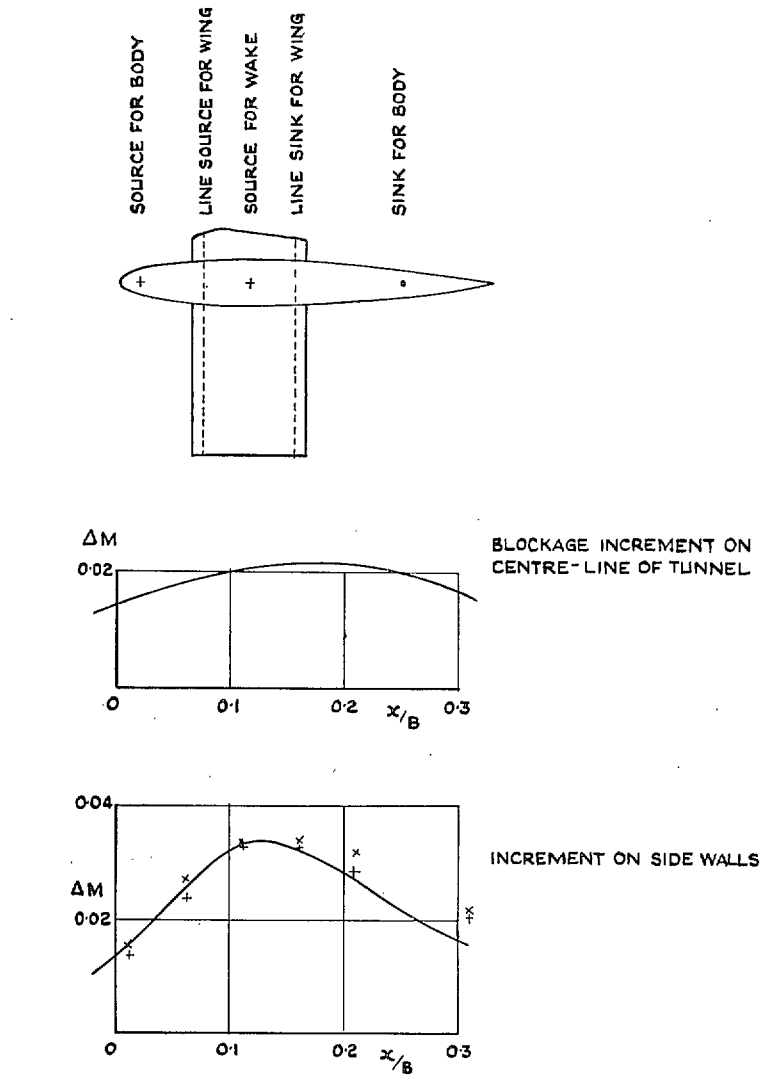

FIG. 33. Comparison of measured and calculated longitudinal distribution of velocity increment due to a wing and body.

(52308) Wt. 15/680 K.9 7/53 Hw

PRINTED IN GREAT BRITAIN

Publications of the Aeronautical Research Council

ANNUAL TECHNICAL REPORTS OF THE AERONAUTICAL RESEARCH COUNCIL (BOUND VOLUMES)

1936 Vol. I. Aerodynamics General, Performance, Airscrews, Flutter and Spinning. 40*s.* (40*s.* 9*d.*)
Vol. II. Stability and Control, Structures, Seaplanes, Engines, etc. 50*s.* (50*s.* 10*d.*)

1937 Vol. I. Aerodynamics General, Performance, Airscrews, Flutter and Spinning. 40*s.* (40*s.* 10*d.*)
Vol. II. Stability and Control, Structures, Seaplanes, Engines, etc. 60*s.* (61*s.*)

1938 Vol. I. Aerodynamics General, Performance, Airscrews. 50*s.* (51*s.*)
Vol. II. Stability and Control, Flutter, Structures, Seaplanes, Wind Tunnels, Materials. 30*s.* (30*s.* 9*d.*)

1939 Vol. I. Aerodynamics General, Performance, Airscrews, Engines. 50*s.* (50*s.* 11*d.*)
Vol. II. Stability and Control, Flutter and Vibration, Instruments, Structures, Seaplanes, etc. 63*s.* (64*s.* 2*d.*)

1940 Aero and Hydrodynamics, Aerofoils, Airscrews, Engines, Flutter, Icing, Stability and Control, Structures, and a miscellaneous section. 50*s.* (51*s.*)

1941 Aero and Hydrodynamics, Aerofoils, Airscrews, Engines, Flutter, Stability and Control, Structures. 63*s.* (64*s.* 2*d.*)

1942 Vol. I. Aero and Hydrodynamics, Aerofoils, Airscrews, Engines. 75*s.* (76*s.* 3*d.*)
Vol. II. Noise, Parachutes, Stability and Control, Structures, Vibration, Wind Tunnels. 47*s.* 6*d.* (48*s.* 5*d.*)

1943 Vol. I. (*In the press.*)
Vol. II. (*In the press.*)

ANNUAL REPORTS OF THE AERONAUTICAL RESEARCH COUNCIL—

1933–34	1*s.* 6*d.* (1*s.* 8*d.*)	1937	2*s.* (2*s.* 2*d.*)
1934–35	1*s.* 6*d.* (1*s.* 8*d.*)	1938	1*s.* 6*d.* (1*s.* 8*d.*)
April 1, 1935 to Dec. 31, 1936.	4*s.* (4*s.* 4*d.*)	1939–48	3*s.* (3*s.* 2*d.*)

INDEX TO ALL REPORTS AND MEMORANDA PUBLISHED IN THE ANNUAL TECHNICAL REPORTS, AND SEPARATELY—

April, 1950 - - - - R. & M. No. 2600. 2*s.* 6*d.* (2*s.* 7½*d.*)

AUTHOR INDEX TO ALL REPORTS AND MEMORANDA OF THE AERONAUTICAL RESEARCH COUNCIL—

1909–1949. R. & M. No. 2570. 15*s.* (15*s.* 3*d.*)

INDEXES TO THE TECHNICAL REPORTS OF THE AERONAUTICAL RESEARCH COUNCIL—

December 1, 1936 — June 30, 1939.	R. & M. No. 1850.	1*s.* 3*d.* (1*s.* 4½*d.*)
July 1, 1939 — June 30, 1945.	R. & M. No. 1950.	1*s.* (1*s.* 1½*d.*)
July 1, 1945 — June 30, 1946.	R. & M. No. 2050.	1*s.* (1*s.* 1½*d.*)
July 1, 1946 — December 31, 1946.	R. & M. No. 2150.	1*s.* 3*d.* (1*s.* 4½*d.*)
January 1, 1947 — June 30, 1947.	R. & M. No. 2250.	1*s.* 3*d.* (1*s.* 4½*d.*)
July, 1951.	R. & M. No. 2350.	1*s.* 9*d.* (1*s.* 10½*d.*)

Prices in brackets include postage.

Obtainable from

HER MAJESTY'S STATIONERY OFFICE

York House, Kingsway, London, W.C.2; 423 Oxford Street, London, W.1 (Post Orders: P.O. Box 569, London, S.E.1); 13a Castle Street, Edinburgh 2; 39, King Street, Manchester, 2; 2 Edmund Street, Birmingham 3; 1 St. Andrew's Crescent, Cardiff; Tower Lane, Bristol 1; 80 Chichester Street, Belfast, or through any bookseller